Plume-driven plumbing and crustal formation in Iceland

Richard M. Allen,[1,2] Guust Nolet,[1] W. Jason Morgan,[1] Kristín Vogfjörd,[3] Meredith Nettles,[4] Göran Ekström,[4] Bergur H. Bergsson,[3] Pálmi Erlendsson,[3] G. R. Foulger,[5] Steinunn Jakobsdóttir,[3] Bruce R. Julian,[6] Matt Pritchard,[5] Sturla Ragnarsson,[3] and Ragnar Stefánsson[3]

Received 23 April 2001; revised 31 December 2001; accepted 4 January 2002; published 22 August 2002.

[1] Through combination of surface wave and body wave constraints we derive a three-dimensional (3-D) crustal *S* velocity model and Moho map for Iceland. It reveals a vast plumbing system feeding mantle plume melt into upper crustal magma chambers where crustal formation takes place. The method is based on the partitioned waveform inversion to which we add additional observations. Love waves from six local events recorded on the HOTSPOT-SIL networks are fitted, S_n travel times from the same events measured, previous observations of crustal thickness are added, and all three sets of constraints simultaneously inverted for our 3-D model. In the upper crust (0–15 km) an elongated low-velocity region extends along the length of the Northern, Eastern and Western Neovolcanic Zones. The lowest velocities (−7%) are found at 5–10 km below the two most active volcanic complexes: Hekla and Bárdarbunga-Grímsvötn. In the lower crust (>15 km) the low-velocity region can be represented as a vertical cylinder beneath central Iceland. The low-velocity structure is interpreted as the thermal halo of pipe work which connects the region of melt generation in the uppermost mantle beneath central Iceland to active volcanoes along the neovolcanic zones. Crustal thickness in Iceland varies from 15–20 km beneath the Reykjanes Peninsula, Krafla and the extinct Snæfellsnes rift zone, to 46 km beneath central Iceland. The average crustal thickness is 29 km. The variations in thickness can be explained in terms of the temporal variation in plume productivity over the last ∼20 Myr, the Snæfellsnes rift zone being active during a minimum in plume productivity. Variations in crustal thickness do not depart significantly from an isostatically predicted crustal thickness. The best fit linear isostatic relation implies an average density jump of 4% across the Moho. Rare earth element inversions of basalt compositions on Iceland suggest a melt thickness (i.e., crustal thickness) of 15–20 km, given passive upwelling. The observed crustal thickness of up to 46 km implies active fluxing of source material through the melt zone by the mantle plume at up to 3 times the passive rate. *INDEX TERMS:* 7220 Seismology: Oceanic crust; 8180 Tectonophysics: Tomography; *KEYWORDS:* oceanic crust, Iceland, tomography, crustal formation, melt migration, hot spot

1. Introduction

[2] The crust of Iceland reflects the history of Mid-Atlantic rifting for the last ∼20 Myr. During this time there have been four separate rift zones, extending across Iceland, responsible for crustal formation as North America and Eurasia drift apart at a rate of ∼2 cm/yr. Oceanic lithosphere and rift systems are remarkably similar around the world, with a constant crustal thickness of 6–7 km [*Muller et al.*, 1997] and an average rift depth of 2.5 km below sea level [*White*, 1997]. Iceland represents one of the most significant anomalies to these observations. Previous studies suggest crustal thicknesses between 2 and 6 times the oceanic norm [*Darbyshire et al.*, 1998; *Weir et al.*, 2001]. In addition, the Iceland rift rises 2 km above sea level, which is 4.5 km above the norm.

[3] Iceland is one of the most intensely studied sections of oceanic crust in the world. This is primarily for the subaerial exposure of a mid-ocean rift allowing fuller access to the associated processes, but also due to its location in the center of one of the classic hot spot signatures associated with mantle plumes by *Morgan* [1971]. The result is an

[1]Department of Geosciences, Princeton University, Princeton, New Jersey, USA.
[2]Now at Department of Geology and Geophysics, University of Wisconsin-Madison, Madison, Wisconsin, USA.
[3]Vedurstofa Íslands, Reykjavik, Iceland.
[4]Department of Earth and Planetary Sciences, Harvard University, Cambridge, Massachusetts, USA.
[5]Department of Geological Sciences, University of Durham, Durham, UK.
[6]U.S. Geological Survey, Menlo Park, California, USA.

0148-0227/02/2001JB000584$09.00

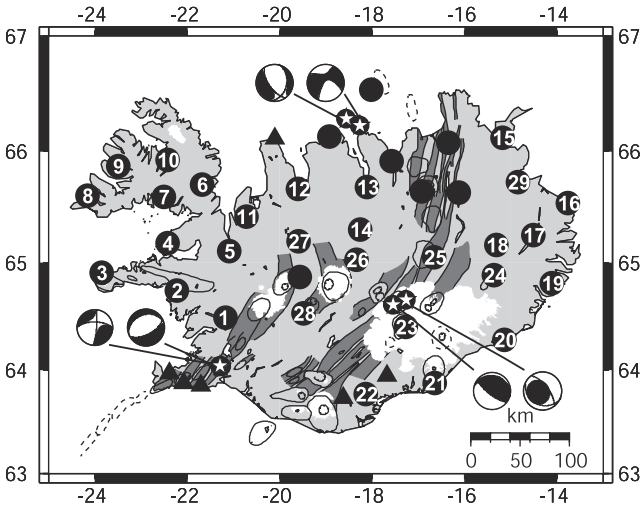

Figure 1. Location map for this study. The numbered circles are HOTSPOT broadband IRIS-PASSCAL stations. They are supplemented by stations from the permanent SIL network operated by Vedurstofa Íslands, represented as unnumbered solid circles for broadband stations and triangles for short-period stations. The combined networks cover the entirety of Iceland with a typical station spacing of 50 km. The location of the six events used are indicated as star filled circles, the associated CMT solutions are adjacent. The land surface is gray, and the glaciers are white. The darker, solid gray streaks are fissure swarms which delineate the Western and Eastern Neovolcanic Rift Zones in southern Iceland and the Northern Neovolcanic Rift Zone in the north. The elliptical features are central volcanoes; central calderas are indicated with hatched lines.

extensive set of geophysical observations and associated interpretations leading to a highly controversial debate over the last four decades.

[4] In one of the first seismic studies of the Icelandic crust, *Bàth* [1960] divided his 28 km thick crust into three constant velocity layers, the compressional-wave speed (V_P) of the lowermost 10 km being 7.4 km/s. Two years later, *Tryggvason* [1962] derived a velocity model for Iceland and ~1000 km of the Mid-Atlantic Ridge to the south from Love and Rayleigh wave dispersion curves. In his model, a 10 km thick crust lies above mantle with a V_P of 7.4 km/s. These two early studies highlight the progression of interpretations which was to follow. While the observations of seismic velocity remained fairly consistent, the interpretation of the velocities created much controversy.

[5] Two models of the Icelandic crust have been dominant. The thin-hot-crustal model interpreted ~7.4 km/s velocities as low-velocity uppermost mantle associated with the highly volcanic nature of Iceland [*Tryggvason*, 1962; *Palmason*, 1971; *Angenheister et al.*, 1980]. This model was supported by observations of a high temperature gradient in near-surface boreholes [*Palmason*, 1973]. In addition, electrical resistivity observations beneath northeast Iceland indicated a high conductivity layer at 10–20 km depth [*Beblo and Bjornsson*, 1980]. This layer was interpreted as being a partially molten uppermost mantle, consistent with the model of a low-velocity mantle.

[6] Although the alternative thick-cold-crustal model has its origins with *Bàth* [1960] and remained within the range of interpretations [*Zverev et al.*, 1977], it only started to become the prevalent interpretation during the 1990s. *Bjarnason et al.* [1993] observed *PmP* reflections along a 2-D seismic line in southwestern Iceland which placed the Moho at 20–24 km. Seismic attenuation studies in western [*Menke and Levin*, 1994] and southwestern [*Menke et al.*, 1995] Iceland give high values of Q (typically $Q_P = 200–300$, $Q_S = 150–600$), which rules out the presence of large expanses of partial melt. More recent crustal studies have converged on the thick-cold-crustal model, placing the crustal thickness between 15 and 43 km [*Staples et al.*, 1997; *Darbyshire et al.*, 1998; *Menke et al.*, 1998; *Weir et al.*, 2001].

[7] Here we present the results of a fully 3-D study of the Icelandic crustal structure. Our S velocity model is derived primarily from local surface wave observations, but also satisfies S_n travel time constraints and previous observations of crustal thickness. The 0.03–0.1 Hz frequency window used in our analysis does not allow us to image structures on a scale less than ~50 km horizontally, and we therefore cannot expect to image some of the details observed on the previous 2-D controlled source lines. However, we are able to image crustal structure as a whole, including Moho depth, in a consistent fashion across Iceland. In addition to providing a complete map of crustal thickness variations, our model reveals a vast plumbing system through which the mantle plume feeds Icelandic crustal formation.

2. Data Set

2.1. The HOTSPOT Experiment

[8] The primary data source for this study is the HOTSPOT experiment. This was a collaborative undertaking between Princeton University, University of Durham, Vedurstofa Íslands (The Icelandic Meteorological Office) and the U.S. Geological Survey. Thirty-five portable broadband instruments were provided by the Incorporated Research Institutions for Seismology-Program for Array Seismic Studies of the Continental Lithosphere (IRIS-PASSCAL) program to be deployed across Iceland from July 1996 till July 1998. Thirty of these instruments were deployed in the HOTSPOT network spanning the entirety of the island, shown on Figure 1 as numbered circles. Stations in coastal regions were typically deployed in low-use or disused buildings providing shelter, power and a low noise environment. In order to maintain even coverage, stations were also deployed in the often desolate interior. Here, mountaineering club huts were used to provide shelter and club members were keen to assist with station deployment and maintenance. Power was provided by large battery packs and solar panels.

[9] The remaining five IRIS-PASSCAL instruments were deployed at Southern Iceland Lowlands (SIL) network sites. The SIL network is a permanent facility operated by Vedurstofa Íslands primarily to monitor earthquake hazard. This network consists of more than 30 stations, both broadband and short-period, concentrated in the north and southwest, both regions of high population and hazard. Figure 1 shows the 13 SIL stations we use in this study. The 7 solid

Table 1. Event Parameters for the Six Local Events on Iceland

Date	Time, UT	Lat. °N	Long. °W	Depth, km	M_{rr}	$M_{\theta\theta}$	$M_{\phi\phi}$	$M_{r\theta}$	$M_{r\phi}$	$M_{\phi\theta}$	Scale, N m	Rise-time, X
29 Sept. 1996	1048:18.157	64.66	17.27	3.6	4.94	−3.26	−1.67	−1.05	3.81	−0.07	10^{17}	5
29 Sept. 1996	1339:13.781	64.617	17.548	1.1	2.10	−1.74	−0.36	2.58	−2.05	1.02	10^{17}	0
22 July 1997	1621:40.176	66.287	18.394	3.5	−2.92	−0.89	3.81	−1.61	1.38	−1.22	10^{16}	0
24 Aug. 1997	0304:22.078	64.036	21.268	5.2	−3.78	3.22	0.56	−1.82	−0.97	1.53	10^{16}	0
20 Sept. 1997	1551:49.564	66.233	18.296	4.2	−0.20	−2.01	2.21	1.10	0.79	−1.68	10^{16}	0
4 June 1998	2136:53.761	64.036	21.289	4.4	−0.52	0.38	0.14	−0.09	−0.78	1.74	10^{17}	0

circles are the broadband instruments, which provide both surface wave data and crustal body wave phases, while the 6 triangles are short-period instruments, which provide only body wave phases. As can be seen in Figure 1, the HOTSPOT network (numbered circles) was designed to complement the SIL network to give even coverage across Iceland with a typical station spacing of 50 km.

[10] Thirty of the thirty-five PASSCAL instruments were Guralp CMG3-ESP seismometers with a flat response proportional to velocity between 0.03 and 10 Hz. There were also four Guralp CMG-40T, and one Guralp CMG-3T instruments. Each was connected to a DAS digitizer which wrote continuous 20 sample per second data to 0.5 or 1 Gb disks, and triggered events at 100 sps. With this capacity, disks filled every 1–4 months, requiring a station visit. While the current explosion in disk size could make such frequent visits obsolete, it is worth noting the importance of station visits to ensure full operation; several HOTSPOT stations failed during the experiment but data loss was minimized by regular station visits and checks. Data from the disks were processed to generate SEED volumes using PASSCAL database software and are now available to the community from the IRIS Data Management Center via the usual data request tools.

[11] Data quality from the network is high despite its portable nature. Many stations were placed on concrete basement slabs in cellars or barns, others on basement rock. In some cases, however, this was not possible and stations were buried at a depth of 1 m in the surface sediment. It was not possible to discern differences in data quality due to this variation. *Allen et al.* [1999, Figure 2] illustrate this, comparing broadband arrivals at the three HOTSPOT stations closest to BORG, a borehole station belonging to the Global Seismic Network (GSN). The data quality is comparable at all four stations.

2.2. Useful Events

[12] During the 2-year duration of the HOTSPOT experiment there were six earthquakes on or just offshore Iceland strong enough to provide surface waves useful for our study. Event parameters are provided in Table 1.

[13] They are all listed in the National Earthquake Information Center Preliminary Determination of Epicenters (NEIC PDE) catalog with body wave magnitudes greater than or equal to 4.5. Large magnitudes are needed to provide enough energy at low frequencies to overcome the microseismic noise levels. The event locations and moment tensors are shown in Figure 1. The six events are in three locations, the Hengill complex in the southwest, the Bárdarbunga-Grímsvötn complex beneath the Vatnajökull ice cap in central Iceland, and in the Tjörnes Fracture Zone to the north of Iceland. All of the place names used here are located on the map in Figure 2

[14] Focal mechanisms and source parameters for the two largest events are available from the Harvard centroid moment tensor (CMT) catalog but have been reanalyzed here with all data currently available; the solutions obtained are similar to those in the catalog. Four events are too small for standard CMT analysis, the source parameters used here were determined using a modified CMT method similar to that described by *Arvidsson and Ekström* [1998], which fits first arriving surface waves at periods of 20–150 s. Dispersion of the fundamental mode at periods in the range 40–150 s is predicted using the global phase velocity maps of *Ekström et al.* [1997], while dispersion at shorter periods is predicted from the crustal model of *Mooney et al.* [1998]. Using the intermediate-period surface waves greatly increases the signal-to-noise ratio for the smaller earth-

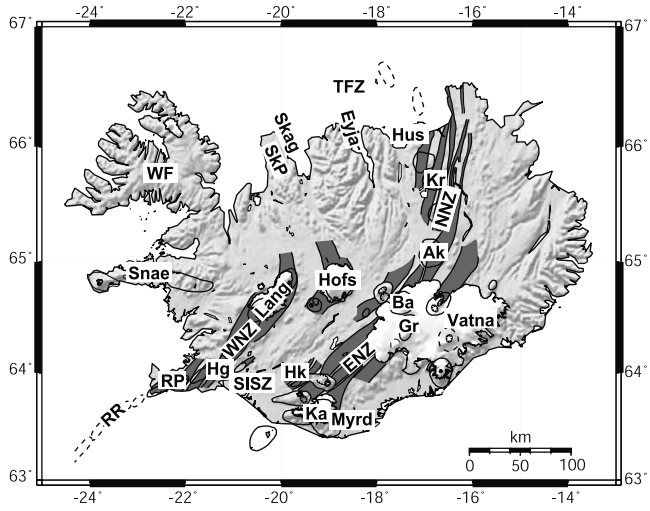

Volcanoes
Ak Askja
Ba Bardarbunga
Gr Grimsvotn
Hk Hekla
Hg Hengill
Ka Katla
Kr Krafla

Glaciers
Hofs Hofsjokull
Lang Langjokull
Myrd Myrdalsjokull
Vatna Vatnajokull

Tectonic/other
ENZ Eastern Neovolcanic Zone
Eyjaf Eyjafjordur
Hus Husavik
NNZ Northern Neovolcanic Zones
RP Reykjanes Peninsula
RR Reykjanes Ridge
Skag Skagafjordur
SkP Skagi Peninsula
Snae Snaefellsnes
SISZ Southern Iceland Seismic Zone
TFZ Tjornes Fracture Zone
WF Westernfjords
WNZ Western Neovolcanic Zone

Figure 2. Location map listing all the volcanoes, glaciers and tectonic features referred to in this paper.

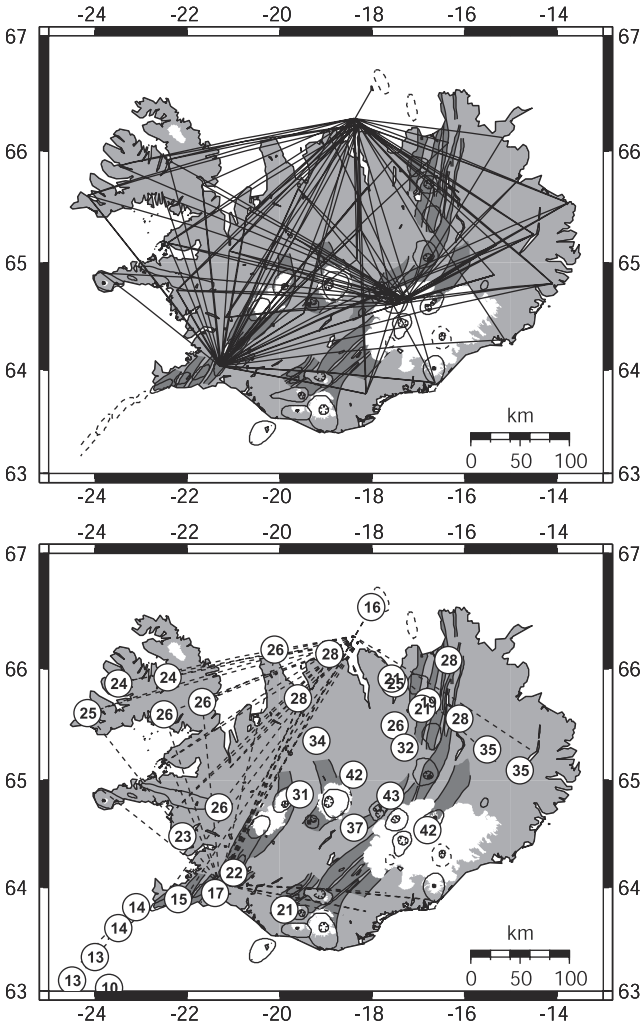

Figure 3. Constraint maps for our study. The primary constraint set consists of 128 local Love waves, their source-station paths are shown on the top map. The bottom map shows the S_n paths (dashed lines) and the point constraints (white circles showing the crustal thickness in km). Note that we were not able to identify S_n for paths beneath central Iceland.

quakes, allowing us to constrain the source parameters for these events. Both HOTSPOT and GSN data are included in the surface wave inversions, and though the response of the PASSCAL instruments falls off rapidly toward longer periods, clear signal is present for many of the events at periods as long as 40 s. Some of the events have a highly non-double-couple nature (see Figure 1); these are discussed in more detail by *Nettles and Ekström* [1998].

3. The Partitioned Waveform Inversion Plus

[15] Our crustal model is derived from three independent sets of constraints: Love waves, S_n travel times, and previous observations of Moho depth, included as constraints on crustal thickness at point (latitude, longitude) locations. We will refer to the latter as point constraints. The surface waves are the primary source of crustal velocity structure information. We choose to use Love rather than Rayleigh waves in anticipation of the application of this model to correct teleseismic *S* arrival travel times. The measurement of both the surface waves and the body wave phases on the transverse component provides consistent measurement of *SH* velocities. S_n provides information about the uppermost mantle velocity in addition to crustal thickness. Finally, the point constraints allow recovery of shorter wavelength Moho variations than would be possible using just the surface waves; they come from controlled source experiments and receiver function analyses. All three sets of constraints are simultaneously inverted for crustal structure.

3.1. Waveform Fitting

[16] The first step of the partitioned waveform inversion (PWI) is waveform fitting. Each of our recorded waveforms is processed independently to obtain a 1-D path-averaged velocity model. The approach was introduced by *Nolet* [1990], and the specifics of the optimization problem we solve are detailed by *van der Lee and Nolet* [1997]. We

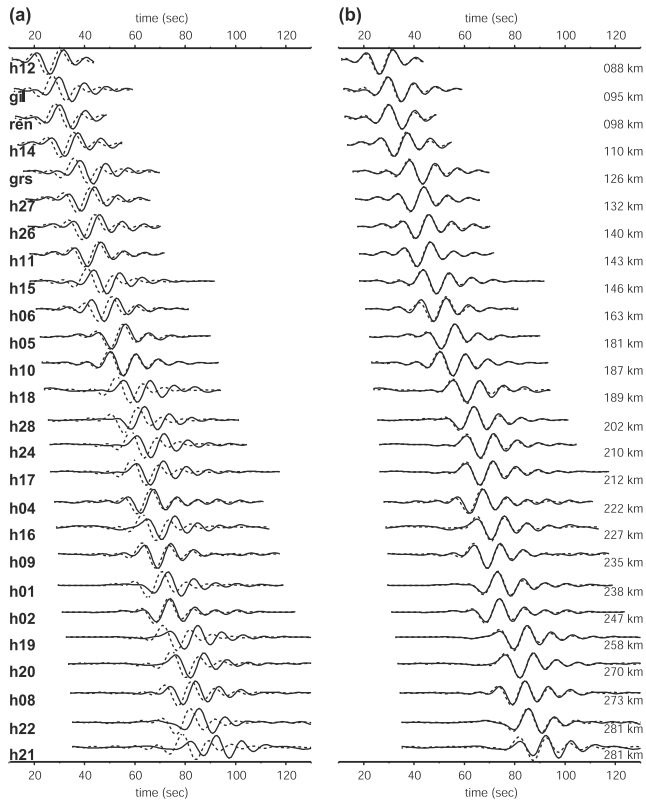

Figure 4. Comparison of initial and final 1-D waveform fits for the 22 July 1997 event. The waveforms are ordered with increasing epicentral distance. (a) The solid line is the observed seismogram; dashed line is the synthetic calculated from the source parameters and an initial radial velocity model using mode summation. (b) Again the solid line is the observed seismogram; the dashed line is the best fit synthetic calculated from our best 1-D path-averaged velocity model for each waveform. The sum of the misfits for all 128 Love waves is reduced by 88% in this step. The misfit for the worst fitting waveform shown (h21, at the greatest epicentral distance) is 0.53; 125 of the waveforms have lower misfits than this.

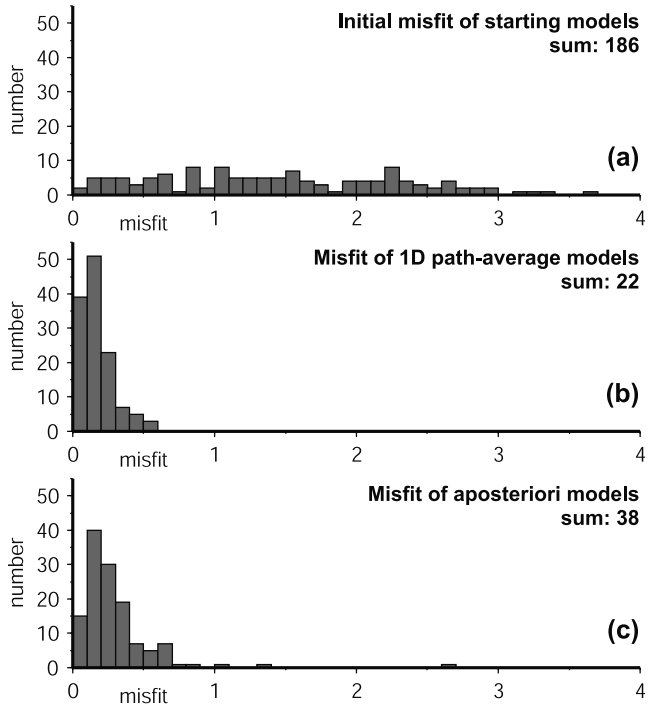

Figure 5. Histograms of the misfit for each waveform. (a) Misfit distribution of initial synthetic fits using our best guess starting models. (b) Misfit after obtaining the best fit to 1-D path-averaged model. (c) Misfit of a posteriori synthetics calculated from the final 3-D crustal model ICECRTb. The misfit reduction from initial to 1-D models is 88%, from initial to a posteriori is 80%.

minimize the misfit between our data and a synthetic seismogram calculated from the earthquake source parameters and an Earth model using mode summation. Using the WKBJ approximation, the synthetic is expressed in terms of the average wave number along the path. For each waveform we choose an appropriate 1-D starting model for which we compute the phase velocity for 20 modes. Perturbations to the wave number are related to variations in the starting model using Frechet derivatives [*Takeuchi and Saito*, 1972] and these are used to compute waveform derivatives. The effect of Moho variations is included in the calculation of the wave number perturbation as described by *Das and Nolet* [1995].

[17] The nonlinear nature of the waveform fitting process requires that we have good starting models. We combined information from previous wide-angle studies [*Bjarnason et al.*, 1993; *Staples et al.*, 1997; *Darbyshire et al.*, 1998] (taking V_P and V_P/V_S estimates) with inversions of group velocity observations from our data to develop the following scheme for generating initial 1-D velocity models, one for each waveform. V_S is fixed at the surface to 2.25 km/s, it then increases linearly to 3.75 km/s at 5 km depth (a velocity gradient of 0.3 s^{-1}). At 5 km there is a significant change in velocity gradient: the velocity increases linearly from 3.75 km/s at 5 km to 3.85 km/s at the Moho (i.e. the velocity gradient varies between 0.005 s^{-1} and 0.003 s^{-1} depending on the depth of the Moho). The velocity jumps from 3.85 km/s at the base of the crust to 4.1 km/s in the uppermost mantle. Below the Moho the velocity gradient is fixed at 0.004 s^{-1}. We found that the waveform fits deteriorated significantly when there was no velocity step at the Moho. This aspect of the velocity structure is also supported by observations of *PmP* reflections [e.g. *Bjarnason et al.*, 1993; *Staples et al.*, 1997]. Higher velocities in the mantle lead to unacceptable misfits between the synthetics and recorded waveforms.

[18] For each path we choose a background model with appropriate Moho depth. Wide-angle seismic studies indicate a significant variation in crustal thickness from 15 km [*Weir et al.*, 2001] to 43 km [*Darbyshire et al.*, 1998]. *Menke*'s [1999] compilation of thicknesses suggests that assuming isostatic equilibrium in Iceland is a reasonable first approximation. We use the best fit line to the compiled crustal thickness observations and corresponding elevation data to estimate crustal thickness across Iceland from the topography. We then choose the initial Moho depth to be the average crustal thickness along the waveform path using this estimate. A concern in the waveform fitting method is the possible trade-off between Moho depth and uppermost mantle velocity. We tested the sensitivity of our waveform fits to this tradeoff by using different starting models for one given path. Starting models with the Moho at 20, 25, 30 and 35 km were used. After waveform fitting, the Moho depth was found to be 27, 28, 28 and 28 km, respectively, indicating a high sensitivity to the path-averaged crustal thickness, minimal effects of the trade-off, and insensitivity to the starting model parameters.

[19] We fit a total of 128 transverse component seismograms, for waves along the paths shown in Figure 3. We select a time window corresponding to group velocities typically between 2.0 and 8.0 km/s for fitting. The quality of the fit is defined by the misfit function, $F(\gamma)$, which is minimized during waveform fitting. It is defined as

$$F(\gamma) = \int w^2(t)[\mathbf{R}d(t) - \mathbf{R}s(t,\gamma)]^2 dt, \qquad (1)$$

where $d(t)$ is the waveform data, $s(t, \gamma)$ is the synthetic calculated from the model parameters γ, $\mathbf{R}$ is a filtering and windowing operator, and $w(t)$ is a weighting function inversely proportional to the amplitude of the waveform envelope applied to enhance the lower amplitude higher mode energy.

[20] One of the strengths of the partitioned waveform inversion is that the synthetic waveforms are compared to the data in the time domain. This allows identification of data contaminated by significant multipathing effects, such waveforms were discarded. Good fits were obtained in the frequency window 0.03–0.1 Hz; at higher frequencies scattered energy did become significant. This frequency window gives us resolution through the crust and into the uppermost mantle. Another source of erroneous velocity structure in analyses of this type are errors in the event location. The similar location of pairs of events in this study allows a test for this problem. The path-averaged models for near-identical paths (i.e., from an event pair to a single station) must be similar, any significant difference would indicate an effect of event source parameters. Using the CMT source parameters derived from GSN and HOTSPOT data we found an excellent match between the velocity constraints from similar paths.

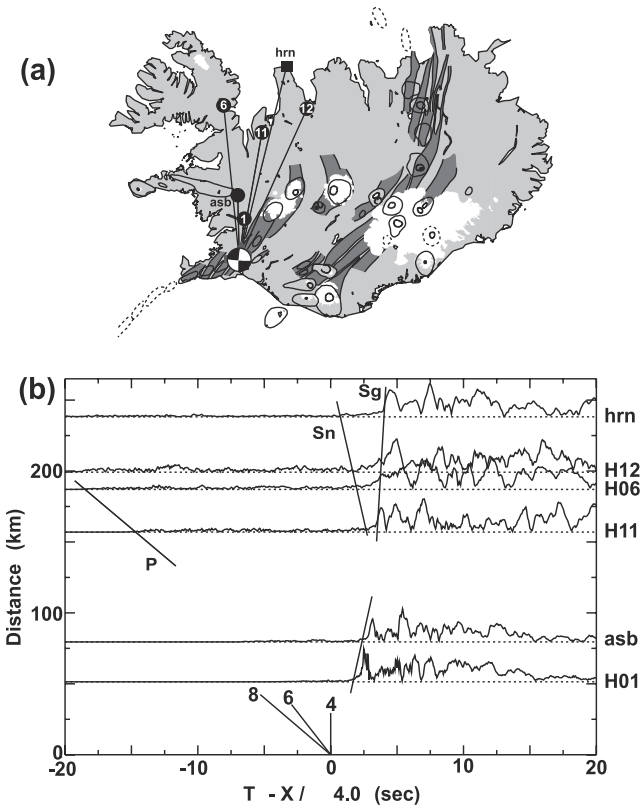

Figure 6. Example of S_n picks and illustration of our approach. (a) Map of the paths for the waveforms shown in Figure 6b. We select groups of stations within some range of azimuths when plotting record sections. (b) Record section showing waveforms as a function of distance from the event. A reduction velocity of 4 km/s has been applied. We plot the envelopes (instantaneous amplitudes) of the transverse components in order to identify S_n and S_g.

[21] Examples of the fits for the event on 22 July 1997 are shown in Figure 4, the data is represented by the solid line. The dashed line in Figure 4a shows the initial synthetic calculated from the chosen starting model. In Figure 4b the dashed line is the synthetic for the best fit 1-D path-averaged model. The 22 July event was located in the Tjörnes Fracture Zone (Figure 1 and Table 1); the poorest fit is at station h21, which is the farthest from the event. The misfit for the 1-D model at this station (Figure 4b) is 0.53– 125 of the 128 Love waves have better fits than this. As we shall see in the next section, this path runs through the most anomalous portion of the Icelandic crust, making it one of the most difficult waveforms to fit. Here, where the crust and mantle change so markedly, the variations to the average 1-D model are most significant. To illustrate the improvement in the waveform fits, Figure 5a shows a histogram of the misfit values for the initial models, while Figure 5b shows the misfit for the 1-D path-averaged models. The reduction in the sum of the misfits is 88%.

3.2. S_n Travel Times

[22] S_n is the head wave which travels along the underside of the Moho. Its travel time is sensitive to both the velocities along the path and the Moho depth. The purpose of including this data set was to provide additional independent constraints on uppermost mantle velocities. Perturbations in the travel time, δt, are related to variations in S velocity, $\delta\beta$, using the well-known integral:

$$\delta t = -\int_{\text{path}} \frac{\delta\beta}{\beta^2} ds, \tag{2}$$

where β is the background model S velocity. Neglecting second-order contributions, the travel time perturbation due to a change in Moho depth is given by:

$$\delta t = \delta H \left[\frac{1}{\beta_c^2} - \frac{1}{\beta_m^2} \right]^{\frac{1}{2}}, \tag{3}$$

where δH is the perturbation in Moho depth and β_c and β_m are the lowermost crust and uppermost mantle S velocities, respectively. We use equation (3) twice for each S_n path, once at the source, and once at the receiver end.

[23] The S_n arrival is difficult to identify as it is often low in amplitude; we therefore only include S_n picks that satisfy the following criteria: (1) We select data from stations within some range of azimuths from the event and plot the envelope (instantaneous amplitude) of the transverse component on a record section as shown in Figure 6, (2) We pick S_n only if we see a coherent arrival across the record section with a mantle move out velocity (i.e., greater than 4.0 km/s) and (3) we also see the crustal phase S_g arriving later with a crustal move out velocity.

[24] We looked for S_n arrivals from all six events, a total of 254 waveforms; the 40 S_n paths used in the inversion are shown in Figure 3. Interestingly, we could not identify any useful S_n arrivals from the two events beneath Vatnajökull, nor were they seen on paths which pass beneath the Vatnajökull area (Figure 3). The S_n data set is significant in the northwest third and southern portion of Iceland. In addition to better constraining the mantle velocity beneath these regions they require thinner crust beneath the South Iceland Seismic Zone and the Snæfellsnes rift than the surface waves alone would suggest.

3.3. Point Constraints on Crustal Thickness

[25] We use recent observations of crustal thickness from 2-D wide-angle seismic lines and receiver function studies to supplement our control on Moho depth. Around the extremities of Iceland, such as the east coast and Reykjanes Peninsula, surface wave coverage is poor or nonexistent. In the regions well sampled by surface waves, the effect of point constraint inclusion is to introduce shorter wavelength variations in crustal thickness. Our surface wave data are satisfied equally well with or without the point constraints, as the changes to the average crustal thickness along each path are small. This observation is very encouraging: it means that these two independent data sets are consistent, though we note that along some paths there are few point constraints so we are not able to make this comparison.

[26] The point constraints used are shown in Figure 3 and listed in Tables 2 and 3. We use observations from five recent controlled source wide-angle experiments. The SIST experiment [*Bjarnason et al.*, 1993] in southwest Iceland

Table 2. Point Constraints on Crustal Thickness Taken From Wide-Angle Experiments[a]

Latitude	Longitude	Crustal Thickness, km	Experiment and Position on Line
66.17	−20.1	25.5	ICEMELT: −120 km
65.74	−19.6	28.3	ICEMELT: −80 km
65.36	−19.2	34.4	ICEMELT: −40 km
65.05	−18.4	41.7	ICEMELT: 0 km
64.86	−17.6	43.3	ICEMELT: 40 km
64.54	−16.8	42.2	ICEMELT: 80 km
65.87	−17.5	24.7	FIRE: −40 km
65.71	−16.8	19.4	FIRE: 0 km
65.56	−16.1	27.8	FIRE: 40 km
65.28	−15.5	35.0	FIRE: 80 km
65.09	−14.8	35.0	FIRE: 120 km
64.48	−22.1	23.2	SIST: 820 km
64.14	−21.0	22.3	SIST: 760 km
63.79	−19.9	21.2	SIST: 690 km
63.95	−21.4	17.0	RISE: A120 km
63.89	−22.2	15.2	RISE: A80 km
63.81	−23.1	13.7	RISE: A40 km
63.61	−23.5	14.0	RISE: B120 km
63.33	−24.0	13.3	RISE: B80 km
63.10	−24.5	12.7	RISE: B45 km
63.03	−23.7	10.1	RISE: D60 km
65.50	−17.5	25.5	B96
65.30	−17.3	31.5	B96

[a]The data come from ICEMELT [*Darbyshire et al.*, 1998], FIRE [*Staples et al.*, 1997], SIST [*Bjarnason et al.*, 1993], RISE [*Weir et al.*, 2001], and B96 [*Menke et al.*, 1998].

crossed the Western Volcanic Zone and South Iceland Seismic Zone. The onshore portion of the FIRE line [*Staples et al.*, 1997] ran across northeast Iceland, crossing the Northern Volcanic Zone and Krafla. B96 [*Menke et al.*, 1998] was a line in northern Iceland adjacent to the Northern Volcanic Zone. The ICEMELT refraction line [*Darbyshire et al.*, 1998] crossed central Iceland from the Skagi Peninsula in the north, through the intersection of the Northern and Eastern Volcanic Zones and beneath Vatnajökull. Finally, the RISE experiment [*Weir et al.*, 2001] ran southwest along the Reykjanes Peninsula from Hengill, and then offshore along the Reykjanes Ridge. In each case we took crustal thickness observations at approximately 40 km intervals along the lines, but only where the authors considered the Moho to be well constrained. In addition, two sets of receiver function results are used. The first comes from 5 HOTSPOT stations in the Westernfjords [*Du and Foulger*, 1999], and the second from 8 broadband SIL stations in north and central Iceland [*Darbyshire et al.*, 2000a], see Figure 3 and Table 3. In both cases there are several estimates of crustal thickness at each station corresponding to different back azimuths. We use a simple average for each station.

3.4. Inversion for 3-D Structure

[27] The 3-D velocity model is parameterized with a Cartesian grid, with vertical and horizontal node spacing of 5 and 10 km, respectively. The Moho variations are parameterized using a grid of nearly equidistant triangular knots [*Wang and Dahlen*, 1995] with the same length scale as the horizontal Cartesian grid spacing. We adopt a background model and invert for deviations from it. For the background model we choose a model defined in the same way as the starting models for the waveform fits, with a Moho depth of 30 km, a reasonable average for Iceland. Note that although we chose different starting models for the waveform fitting, we obtained an absolute velocity model (with uncertainties) from those fits. We then subtract one background model from all the 1-D, absolute velocity models before inverting for the 3-D model.

[28] Before we can combine the three sets of constraints on V_S and crustal thickness we must scale the system to account for the multiple parameter and data types. This is achieved with the model and data covariance matrices, $\mathbf{C}_m$ and $\mathbf{C}_d$, respectively. The model covariance matrix $\mathbf{C}_m$ normalizes the velocity and Moho perturbations so that damping has an equal effect on both parameters. We use a priori estimates for the deviation in velocity and crustal thickness from our background model of 0.185 km/s and 10 km, respectively, based on the size of variations observed.

[29] The data covariance $\mathbf{C}_d$ scales each row of the matrix, controlling the relative importance of each con-

Table 3. Point Constraints From Receiver Function Analyses[a]

Latitude	Longitude	Crustal Thickness, km	Station
65.705	−21.678	25.7	h06
65.598	−22.510	25.7	h07
65.610	−24.161	25.0	h08
65.874	−23.487	24.0	h09
65.927	−22.428	23.7	h10
64.749	−21.326	25.6	asb
64.872	−19.559	30.5	hve
64.560	−18.386	37.0	skr
65.647	−16.915	20.5	ren
66.077	−16.351	27.5	gil
65.918	−17.578	21.0	gra
66.133	−18.915	27.5	sig
66.542	−18.010	16.0	gri

[a]Crustal thicknesses from HOTSPOT ("h") stations come from *Du and Foulger* [1999], the rest are from *Darbyshire et al.* [2000a].

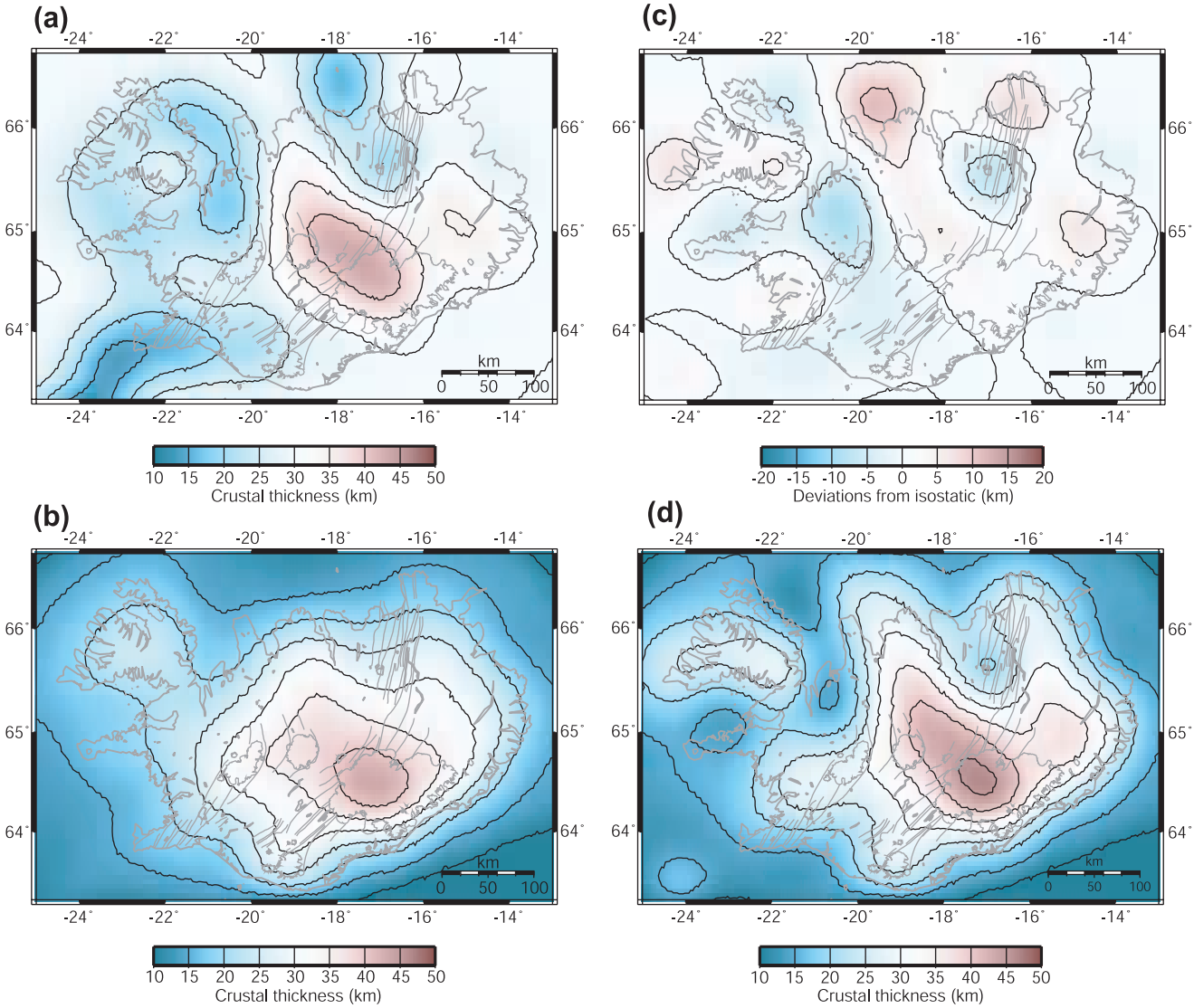

Figure 7. (a) Initial estimate of crustal thickness, from ICECRTa. Crustal thicknesses range between 15 and 44 km. This model is derived from a damped inversion to obtain variations from a background model with a crustal thickness of 30 km. For this reason, unconstrained areas, i.e., offshore with the exception of the Reykjanes Ridge, show a crustal thickness of 30 km. (b) Isostatically predicted crustal thickness map for Iceland calculated from corrected and smoothed elevation. (c) Deviations in crustal thickness from the isostatically predicted values, constrained by our three sets of constraints. The total range of deviations is +11 km (thicker than isostatic) to −7 km. The generally small deviations, <5 km for most of Iceland, indicate that the Icelandic crust is generally in isostatic equilibrium. (d) Crustal thickness variations across Iceland. ICECRTb is obtained by using our various constraints to determine variations from an isostatic model, which is preferable to damping toward a constant thickness crust of 30 km as in ICECRTa. The crustal thickness on Iceland varies between 15 and 46 km. See text for interpretation of these variations.

straint. In our case this scaling factor consists of two components. Firstly, within each of the three constraint sets we must scale according to the relative uncertainties of each datum, which can be estimated in a formal fashion. The scaling we use for our surface wave constraints is derived from the uncertainty estimates in the waveform fitting stage [*van der Lee and Nolet*, 1997]. We estimate the uncertainty in the S_n picks to be 0.2 s based on an assessment of the waveforms. For the point constraints we use the uncertainty estimate made by *Darbyshire et al.* [1998] of ±2 km, though the uncertainty in the receiver functions estimates is probably larger. The second component reflects the relative weight given to each set of constraints, which controls the degree to which each constraint set is satisfied should they contradict one another. We choose weights such that the surface wave and S_n constraints are approximately equally weighted. Initially, we did the same with the point constraints; however, increasing their weight to obtain a closer fit to the point constraints had a minimal effect on the surface wave fits for the reasons given in section 3.3. For

this reason we allowed a higher weighting of the point constraints.

[30] Combining the constraint types and scaling, we obtain the linear system:

$$\mathbf{C}_d^{-\frac{1}{2}}\mathbf{A}\mathbf{C}_m^{\frac{1}{2}}\mathbf{x} = \mathbf{C}_d^{-\frac{1}{2}}\mathbf{d}, \tag{4}$$

where $\mathbf{A}$ is the constraint matrix, $\mathbf{x}$ the nondimensional model and $\mathbf{d}$ the data vector. We obtain the physical model, $\mathbf{m}$, from $\mathbf{x}$ after inversion by simply re-applying $\mathbf{C}_m$:

$$\mathbf{m} = \mathbf{C}_m^{\frac{1}{2}}\mathbf{x}. \tag{5}$$

[31] The approximations implicit in the above constraint set require that the velocity in Iceland varies in a smooth fashion. We therefore specify that $\mathbf{x} = \mathbf{Sn}$, where $\mathbf{S}$ is a smoothing matrix and $\mathbf{n}$ the rough model. The system becomes

$$\mathbf{C}_d^{-\frac{1}{2}}\mathbf{A}\mathbf{C}_m^{\frac{1}{2}}\mathbf{S}\mathbf{n} = \mathbf{C}_d^{-\frac{1}{2}}\mathbf{d}, \tag{6}$$

which we write as

$$\mathbf{H}\mathbf{n} = \mathbf{q}, \tag{7}$$

where $\mathbf{H} = \mathbf{C}_d^{-\frac{1}{2}}\mathbf{A}\mathbf{C}_m^{\frac{1}{2}}\mathbf{S}$ and $\mathbf{q} = \mathbf{C}_d^{-\frac{1}{2}}\mathbf{d}$. We smooth over a disk-shaped elliptical volume which extends 7.5 km from the center point in the vertical direction and 60 km horizontally. The smoothing function weight decreases linearly from the center to the edges of the volume. Compared to the vertical node spacing of 5 km, smoothing is slight in the vertical direction, but we found this small amount to be useful to stabilize the model.

[32] Finally, the system is regularized by damping toward a zero model. The final system of equations we invert is

$$\begin{pmatrix}\mathbf{H}\\ \lambda\mathbf{I}\end{pmatrix}\mathbf{n} = \begin{pmatrix}\mathbf{q}\\ \mathbf{0}\end{pmatrix}, \tag{8}$$

where λ is the damping coefficient determining the strength of damping.

4. Iceland's 3-D Crustal Structure

[33] We start by inverting our constraint sets for 3-D velocity variations from a background model defined as described for the waveform fits with a crustal thickness of 30 km. The resulting crustal thickness map for this model, ICECRTa, is shown in Figure 7a. The damping factor, λ, was chosen to suppress large perturbations but only up to the point where any further damping resulted in unacceptable deterioration of data fit. The data fit was assessed by calculating a posteriori synthetic waveforms and comparing them to the data. A posteriori synthetics were derived from the 3-D velocity model by first calculating average 1-D models for each source-receiver path and then calculating a synthetic using mode summation. The variance, or sum of the misfits, $F(\gamma)$, for all 128 waveforms was used to monitor the extent to which the constraints were satisfied. In the initial waveform fitting step to obtain the 1-D path-averaged models the variance was reduced by 88% with respect to the fit of the initial starting model synthetics. After inversion for 3-D structure the variance reduction was still 80% despite the requirement that all waveforms now be satisfied simultaneously. Inverting for variations to a background model and applying damping assures that we obtain zero perturbation in regions with no constraints. In the case of ICECRTa (Figure 7a), such regions will show the background crustal thickness of 30 km since we have no information about true crustal thickness. This is the case for offshore Iceland with the exception of the Reykjanes Ridge. In regions with few constraints, such as the east coast, velocity anomalies are damped to a greater extent than in the highly constrained regions such as central Iceland. Therefore, when interpreting the ICECRTa velocity anomalies one must be wary of over-interpreting in poorly constrained regions such as the east coast. See Figure 3 to identify unconstrained and poorly constrained regions.

[34] Crustal thickness variations within Iceland (Figure 7a) are large, ranging from 15 km in the southwest and northwest, to more than 40 km beneath central Iceland. Thin crust extends from the Reykjanes Peninsula east beneath the South Iceland Seismic Zone, which accommodates lateral plate motions associated with the ridge jump from the Reykjanes Ridge to the Eastern Volcanic Zone. A strip of thin crust separates the Westernfjords from the rest of Iceland. There is also a tongue of thin crust extending from the north coast beneath the Northern Neovolcanic Zone. The thickest crust corresponds to the area of greatest elevation beneath northwestern Vatnajökull.

4.1. Isostasy in Iceland

[35] The obvious correlation between crustal thickness and elevation leads to the question of isostasy in Iceland. The volcanic formation of Iceland's crust at the Mid-Atlantic Ridge would imply isostasy. We therefore propose to test against our data the hypothesis that Iceland is in Airy-isostatic equilibrium [e.g., *Menke*, 1999].

[36] To obtain a map of topography and bathymetry for comparison (we simply refer to topography from here onward), corrections must be made to the true topography to account for ice thickness and water depth. We use a 2-minute data set [*Smith and Sandwell*, 1997] for the North Atlantic. Ice thickness has been mapped for approximately 50% of Iceland's four major ice sheets: 60% of Vatnajökull, including the thickest parts, and all of Hofsjökull. Where maps are available [*Bjornsson*, 1988] we sample ice thickness on a regular grid at intervals of 10 km. For the remainder of Vatnajökull, Langjökull and Mýrdalsjökull we use a simple quadratic relation between distance from the glacier edge along the flow line and ice thickness [*Paterson*, 1994]. Despite its simplicity we find this relation to be correct to within 10% for the regions where ice thickness has been mapped. Using average crustal, ice and water densities of 2900, 900 and 1050 kg/m^3 we correct the true topography to account for these density variations.

[37] In order to compare elevation and Moho variations on the same wavelength we smooth the corrected topography in the same fashion as the crustal model. We smooth

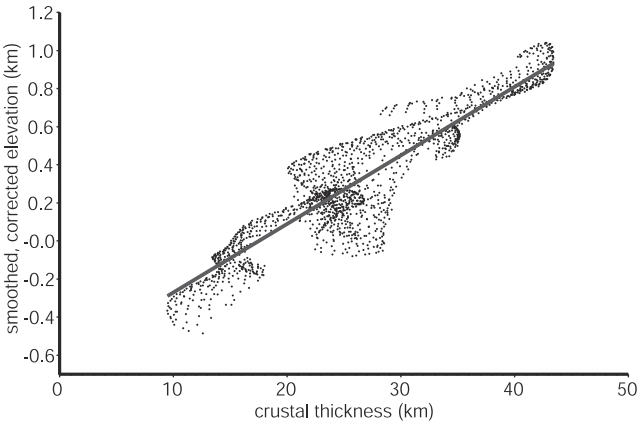

Figure 8. Isostatic relation for the Icelandic crust. We plot the crustal thickness for the most highly constrained points in the model against corrected and smoothed elevation, black dots. The swathes of points are due to smooth variations in crustal thickness and elevation within highly constrained patches of the model. The line represents a linear isostatic relation obtained using L^1 norm linear regression.

with a weighting function defined such that zero weight is given to points at radii greater than 60 km from the point of interest, with the weight increasing linearly with decreasing radius.

[38] Figure 8 shows the relation between topography and the most highly constrained crustal thickness observations from our model (Figure 7a). The swathes of points are not independent but represent smooth variations within the highly constrained patches. There is a small bias toward 30 km thickness due to damping in the inversion. L^1 norm linear regression provides the following isostasy relation illustrated in Figure 8:

$$T = 18 + 28e_s, \tag{9}$$

where T is the crustal thickness and e_s is the appropriately smoothed elevation, both in km. To test the sensitivity of this relation we increased and decreased the degree to which crustal thickness points must be constrained in order to be included in the regression. We find only minor variations in the best-fit isostatic relation. If the relation is expressed $T = c + ge_s$, c is found to vary from 17 to 18 km, and g from 26 to 28. Consideration of the full range of linear relations which give an acceptable fit to the points in Figure 8 provides a more complete estimate of the error. In this case c varies from 17 to 23 km and g from 21 to 28.

[39] This relation implies a relatively small density contrast of 4% across the Moho. *Menke* [1999] estimated the density at the base of the Icelandic crust to be 3060 ± 50 kg/m^3 based on the density and composition of near surface basalts using the compressibilities and thermal expansion coefficients of *Clark* [1966]. Using this lower crustal density we predict a density contrast of 130 ± 30 kg/m^3, a little larger than *Menke's* [1999] own estimate of 89 ± 12 kg/m^3, which was based on crustal thickness observations from wide-angle lines and a three-layer crustal density structure.

[40] Using a relation between V_P and density, *Darbyshire et al.* [2000b] estimate the density range at the base of the Icelandic crust to be 3070 to 3100 kg/m^3 along various seismic profiles. Using a similar isostasy argument, they estimate the average uppermost mantle density to be 3170–3190 kg/m^3, corresponding to an average crust to mantle density contrast of 2 to 4%. Our density contrast of 4% is at the higher end of *Darbyshire et al.'s* [2000b] range, and is larger than *Menke's* [1999] estimate of 3%. This suggests that the average density contrast beneath Iceland is larger than the local contrast observed beneath their respective study regions. Both *Menke* [1999] and *Darbyshire et al.* [2000b] use wide-angle lines which are preferentially located near active neovolcanic zones, where we would expect lower density mantle due to higher temperatures and perhaps the presence of partial melt. However, the small contrast indicates the special nature of the Moho beneath Iceland, which is characterised by a minor change in composition.

4.2. Testing the Isostatic Model

[41] Given our isostatic relation (equation (9)), we predict the crustal thickness from the smoothed and corrected topography to obtain a map of isostatic crustal thickness which varies from 15 to 43 km, as shown in Figure 7b. We use our seismic constraints to determine where the crust is not in isostatic equilibrium by inverting for perturbations from an isostatic starting model, $\mathbf{n}_{iso}$. We modify our linear system (equation (7)) to obtain:

$$\mathbf{H}(\mathbf{n} - \mathbf{n}_{\mathrm{iso}}) = \mathbf{q} - \mathbf{H}\mathbf{N}_{\mathrm{iso}}. \tag{10}$$

We apply the same damping as previously; however, rather than damping relatively unconstrained portions of the model toward a 30 km crust and zero velocity perturbation, we now damp toward an isostatic crustal thickness and zero velocity perturbation.

[42] The seismic constraints show that most of Iceland is within 5 km of isostatic equilibrium. But there are a few deviations from the isostatic model required by the data as shown in Figure 7c. They vary between +11 km (thicker than isostatic) and −7 km, still significantly less variation than is observed in the total crustal thickness across Iceland, about 30 km. The largest anomaly, of +11 km, occurs north of Iceland, extending off the peninsula between Skagafjördur and Eyjafjördur. This peninsula exhibits high topography relative to Skagi Peninsula and the old Snæfellsnes rift zone to the west, and the current rift zone to the east. The northward thickening of the crust relative to the isostatic prediction implies that the crustal thickness remains fairly constant while the topography drops below sea level. Thicker crust is also found in eastern Iceland adjacent to the Færoes-Iceland Ridge. Thinner crust is found beneath Krafla in the Northern Volcanic Zone, and in northwestern Iceland.

4.3. ICECRTb: Our Preferred Crustal Model

[43] Figure 7d shows the absolute crustal thickness for our preferred model ICECRTb. It is the sum of our isostatically predicted crustal thickness and the deviation from isostasy required by the seismic data. The main features remain the same as in ICECRTa (Figure 7a). The thickest

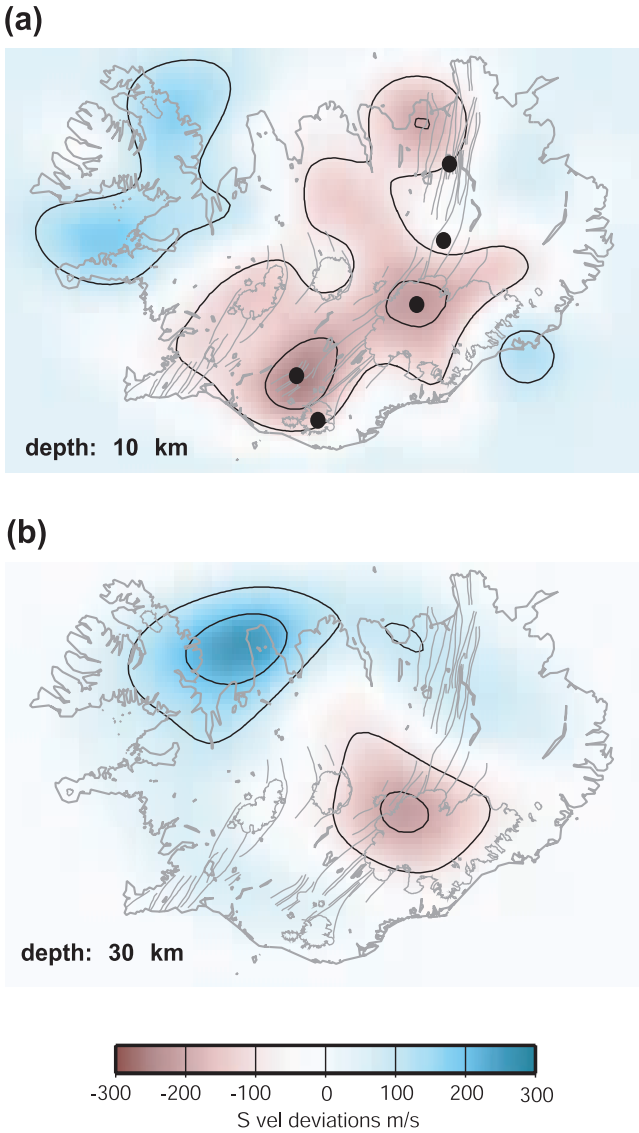

Figure 9. Horizontal sections through the velocity structure of Iceland, ICECRTb, at (a) 10 km depth and (b) 30 km depth. There is no zero contour. The mean velocity anomalies have been subtracted in each case. At 10 km depth, we see elongate low-velocity regions extending along the neovolcanic zones, though there is a gap in the anomaly in the central section of the Northern Neovolcanic Zone corresponding to a region of thin crust. The five main volcanic complexes in terms of activity in historic times are indicated with black circles. The largest anomalies are observed beneath the Hekla and Bárdarbunga-Grímsvötn volcanic complexes, while little or no anomaly is seen beneath Katla, Askja and Krafla. At 30 km depth, low velocities occur in a single circular anomaly with a diameter of ~150 km beneath central Iceland.

crust extends from Vatnajökull north-northwestward toward the high topography and east-northeastward toward the Færoes-Iceland Ridge. Thick crust is also found in the northeast adjacent to the Northern Neovolcanic Zone, and beneath the Western and Eastern Neovolcanic Zones. Tongues of thin crust extend inland from the north down the Northern Neovolcanic Zone, between ridges of thicker crust on either side, and up the Reykjanes Peninsula and across the South Iceland Seismic Zone. There is also an island of thicker crust associated with the Westernfjords; the narrow land bridge between it and the rest of Iceland has some of the thinnest crust, only 15–20 km. Overall, the thickness varies from 15 km on the Reykjanes Peninsula and in northwestern Iceland to 46 km beneath northwestern Vatnajökull.

[44] The variation in crustal thickness is similar to the model of *Darbyshire et al.* [2000b] who used receiver

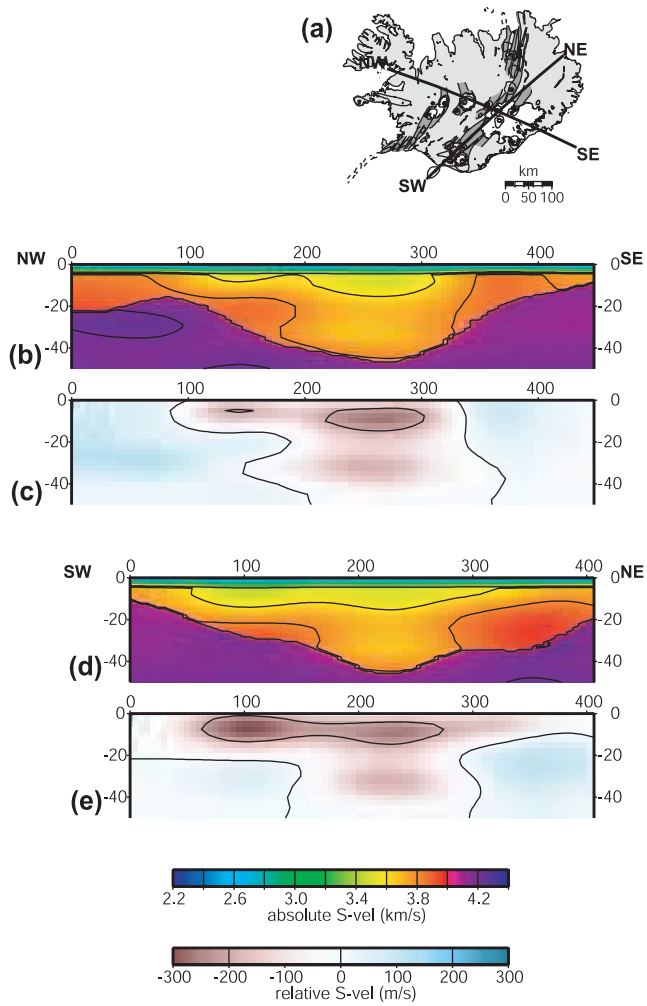

Figure 10. Vertical slices through the velocity structure of Iceland, ICECRTb. Slices are parallel and perpendicular to the main Eastern Neovolcanic Zone. Each slice is shown twice. Figures 10b and 10d show absolute velocity variations which illustrate both the velocity anomalies and crustal thickness variations. Purple colors correspond to mantle velocities. Note the thick crust in central Iceland and the necking to the NW before the thicker crust of the Westernfjords. Figures 10c and 10e are relative velocity anomalies along the same lines and clearly show the communication between the lower crustal low velocities and the horizontal upper crustal low-velocity anomaly which extends up and down much of the ridge.

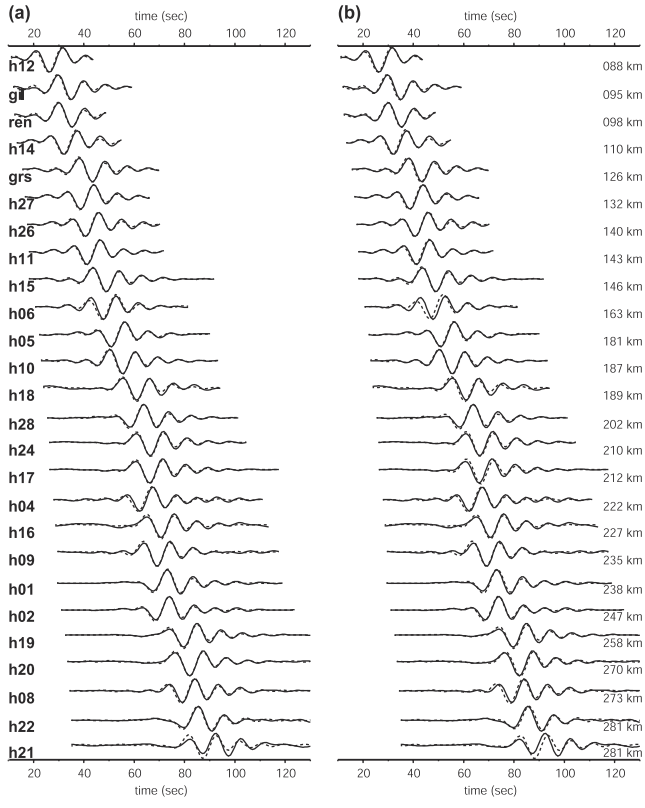

Figure 11. Comparison of recorded data with synthetic waveforms calculated from (a) our 1-D path-averaged models and (b) a posteriori models derived from the 3-D crustal model for the 22 July 1997 event. The data are the solid line; dashed lines represent synthetics. The reduction in the variance is 88% for the 1-D models and 80% for the a posteriori synthetics.

functions and 2-D wide-angle seismic surveys combined with gravity to constrain Moho depth. In their model the thickest crust is also in central Iceland where there Moho depth is 40–41 km corresponding to a crustal thickness of 42–43 km. Their thick crust also extends to the northwest and east. The most significant difference is in the strip of thin crust we resolve in the northwest between the Westernfjords and the body of Iceland. There have been no wide-angle studies in this region which is perhaps why *Darbyshire et al.* [2000b] do not resolve it. Overall there is good agreement between the models.

[45] Horizontal slices through the velocity portion of ICECRTb at depths of 10 and 30 km are shown in Figure 9. For each slice the mean velocity anomaly over the slice (3.72 km/s at 10 km, 3.88 km/s at 30 km) has been subtracted and we show the deviations from this value. The geometry of the anomalies is very different between the two slices, but representative of the difference between the upper and lower crust in Iceland. In the upper crust (Figure 9a), low-velocity regions of −4% extend along most of the neovolcanic zones to a depth of 10–15 km. Larger anomalies, of up to −6% or −0.2 km/s, are observed beneath the Eastern Neovolcanic Zone than beneath the Western Neovolcanic Zone, a difference which correlates with higher levels of volcanic activity at the former. Farther from the active rift zones, crustal velocity anomalies are positive, implying cooler crust. We note that the absence of anomalies off the Reykjanes Peninsula in our model is due to a lack of coverage. In the lower crust, at 30 km depth (Figure 9b), low-velocity anomalies are confined to a single circular region below northwestern Vatnajökull, where they reach −5%. The anomaly is ∼150 km in diameter and is centered below the Bárdarbunga-Grímsvötn Complex, one of the most active volcanic regions in Iceland.

[46] The relationship between the crustal thickness and velocity anomalies is shown in Figure 10, which shows vertical sections parallel and perpendicular to the Eastern Neovolcanic Zone, the most active rift in Iceland. Both the relative velocity anomalies (with respect to the background model) and absolute *S* velocities are shown so that Moho topography is clear. Low velocities in the lower crust correspond to regions of crustal thickening. These low velocities connect with the upper crustal low velocities which then extend along most of the rift. In the section perpendicular to the rift, the upper crustal velocity lows do not extend to the southeast but do extend a little to the northwest, corresponding to the Western Neovolcanic Zone. Parallel to the rift, the upper crustal lows extend along almost the entirety of the section.

[47] To ensure that ICECRTb satisfies our constraints we calculate a posteriori synthetic waveforms; a representative example is shown in Figure 11. As in Figure 4, the data are shown as a solid line. In Figure 11a the dashed lines are the synthetics for the 1-D path-averaged models (as in Figure 4b). In Figure 11b the dashed synthetics are for the 3-D model. As with the 1-D fits the biggest misfit of 0.68 is for station h21, which lies farthest from this event, with the path located across the part of Iceland with the largest crustal variations. 122 of the 128 Love waves have a posteriori misfits better than this, as shown in Figure 5c, which is a histogram of all the waveform misfits. The total reduction in the variance from the starting models is 80%; ICECRTb satisfies the waveform data as well as ICECRTa.

5. Discussion of Crustal Structure

5.1. Ridge-like Upper Crust

[48] To first order, the low-velocity zones in the upper crust (by which we mean the surface to 10–15 km depth), correlate with the neovolcanic zones on Iceland (Figure 9a). The entirety of the Eastern and Western Neovolcanic Zones are underlain by low velocities at this depth. The Northern Neovolcanic Zone correlates with low velocities at the southern end (north of Vatnajökull) and the northern end below Húsavík where the Tjörnes Fracture Zone intersects the neovolcanic zone. The low-velocity region is absent in between, however, including areas beneath Krafla and Askja. The low velocities are most likely due to a combination of rock texture, such as fracturing and faulting, and high temperatures due to their location in an active rift zone. There may also be regions of partial melt.

[49] There are five major volcanic complexes in the Eastern and Northern Neovolcanic Zones, which are the most active rift zones on Iceland. From south to north, they are Katla, Hekla, the Bárdarbunga-Grímsvötn complex

beneath Vatnajökull, Askja and Krafla (Figure 2). There is no simple relationship between these central volcanoes and the imaged velocity anomalies as we image large velocity anomalies beneath only two of the five, while the remaining three are associated with only small anomalies.

[50] When considering the upper crustal anomalies imaged with surface waves it is important to bear in mind the wavelengths in use. The 0.03–0.1 Hz frequency window used corresponds to wavelengths in the 40–120 km range. We therefore cannot expect to image structures with a horizontal extent much smaller than this. It is for this reason that we do not expect to image the shallow crustal magma chambers previously imaged using controlled source methods beneath Katla [*Gudmundsson et al.*, 1994] and Krafla [*Einarsson*, 1978; *Brandsdottir and Menke*, 1992; *Brandsdottir et al.*, 1997]. In both cases the magma chamber lies at a depth of 3 km, is about 1 km thick, and has a lateral extent of between 2 and 10 km. These shallow crustal magma chambers are too small to be imaged in our model. Despite this, the two largest anomalies are centered beneath the two most recently erupting volcanoes, Hekla and Bárdarbunga-Grímsvötn.

[51] The largest anomaly, of −7%, lies at 5–10 km depth beneath Hekla in southern Iceland (Figure 9a). Hekla is one of Iceland's most active volcanoes, erupting at least 18 times since 1104, and five times during the 20th century, including the most recent eruption on Iceland in February 2000. Although no magma chamber has been previously imaged beneath Hekla, estimates of the source depth for the erupted material have been made using a variety of geodetic observations associated with the previous two eruptions in 1980–1981 and 1991. Modeling of ground tilt measurements [*Tryggvason*, 1994] put the source at 5–6 km, while horizontal distance measurements [*Gronvold et al.*, 1983; *Kjartansson and Gronvold*, 1983; *Sigmundsson et al.*, 1992] put the source at 7–10 km depth. Observations of strain variations during the course of the 1991 eruption [*Linde et al.*, 1993] are consistent with a reservoir centroid at a depth of 6.5 km with a radius of 2.5 km. These estimates are consistent with the depth of our imaged anomaly at 5–10 km depth. The volume of the erupted material associated with these events ranged from 0.05 to 0.15 km^3 [*Kjartansson and Gronvold*, 1983; *Sigmundsson et al.*, 1992]. Even a magma chamber with a volume 3 orders of magnitude greater than this would not be imaged by our surface waves. Instead, our results suggest a broad region of high temperatures and possibly partial melt.

[52] There are no geodetic measurements to indicate the magma source depth beneath the Bárdarbunga-Grímsvötn volcanic complex, the location of the second major low-velocity zone in the upper crust (Figure 9a), due to its inaccessibility below several hundred meters of ice [*Bjornsson*, 1988]. It is perhaps reasonable to assume a deep source, however, as the complex sits on top of a low-velocity zone which extends through the entirety of the crust (Figure 9b) and into the mantle [*Allen et al.*, 2002]. Like Hekla, it is also one of the most active volcanic systems in Iceland, and was the most active system during the 20th century, erupting six times, most recently in 1996 and 1998.

[53] The remaining three volcanic complexes, Krafla, Askja and Katla, exhibit a different set of eruptive characteristics and are all located on the edges of our imaged low-velocity zones. First, they all have a shallow, ∼3 km depth, magma source. Seismic imaging [*Einarsson*, 1978; *Brandsdottir and Menke*, 1992; *Brandsdottir et al.*, 1997], and modeling of surface deformation [*Bjornsson et al.*, 1979; *Tryggvason*, 1986; *Arnadottir et al.*, 1998] put the Krafla magma chamber at around 3 km depth. Modeling of surface deformation during the entirety of the 1975 to 1984 rifting event does suggest a deeper magma source in addition to the 3 km deep chamber [*Tryggvason*, 1986; *Arnadottir et al.*, 1998], though given the available ground deformation data it is only possible to determine that its depth is >5 km. There has been no seismic imaging of Askja, but deflation modeling puts the chamber at 1.5–3.5 km depth [*Camitz et al.*, 1995; *Tryggvason*, 1989]. Finally, a magma chamber was imaged beneath Katla by *Gudmundsson et al.* [1994], also at 3 km depth.

[54] The second characteristic distinguishing these three volcanoes is the frequency of eruptions, which is lower than for Hekla and Bárdarbunga-Grímsvötn. There have been only two rifting episodes associated with Krafla during historical times, one in 1724–1729, and the second in 1975–1984 [*Bjornsson et al.*, 1977]. Askja has experienced three eruptions in historic times. The first, in 1875, was the caldera-forming explosion; from 1920 to 1930 there was a sequence of eruptions associated with a rifting event; finally, there was a single eruption in the Dyngjufjöll complex on the flanks of Askja in 1961. Katla, in the south, has been the most active of the three, erupting on an average of 1.5 times a century [*Gudmundsson et al.*, 1994], including once during the 20th century, in 1918.

[55] We propose that the main low-velocity features we image in the upper crust are due to broad regions of high temperature and perhaps partial melt which act as a deep (∼10 km) source for the frequent volcanism associated with Hekla and the Bárdarbunga-Grímsvötn complex. Volcanic activity at Krafla, Askja and Katla is driven by a separate process resulting in small, shallow (∼3 km) magma chambers and less frequent volcanism, which in turn results in a reduction or absence of the thermal halo imaged as low velocities at 5–10 km depth in our model.

5.2. Plume-like Lower Crust

[56] In the lower crust (depths greater than 15 km) low velocities are confined to a single, quasi-circular region with a diameter of ∼150 km (Figure 9b). Figure 12 shows the results of a resolution test designed to test our hypothesis that while the low velocities in the upper crust extend along most of the length of the neovolcanic zones, low velocities in the lower crust are confined to central Iceland only. We conduct a total of nine resolution tests, placing synthetic low velocity anomalies (−0.4 km/s) at 0–15 km, 15–30 km depth and a 12 km Moho anomaly at three locations along the neovolcanic zones. The maps in Figure 12 show the locations of the anomalies. The amplitude of all input velocity anomalies were the same; the recovered anomalies are shown in Figure 12 and recovery is good in all cases. The amplitude loss in the upper crust is smaller than in the lower crust; however, at a given crustal depth the anomalies are recovered equally well all along the neovolcanic zones. In the case of the Moho, there is a variation in amplitude of recovery for the southernmost test. The resolution test demonstrates that if the low velocities in the lower crust

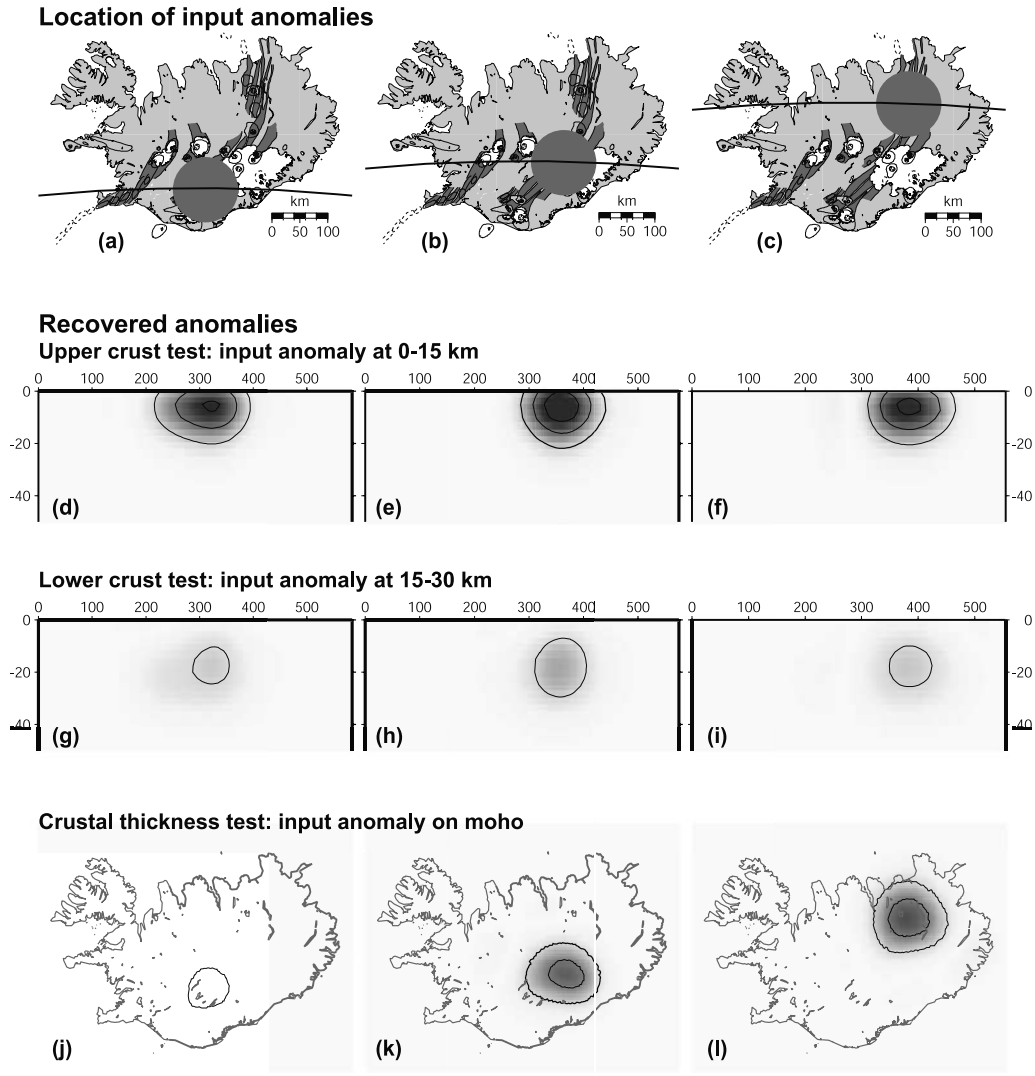

Figure 12. Resolution test. We place synthetic velocity anomalies in the upper and lower crust and on the Moho at (a)–(c) three locations (gray circles) along the rift. (d)–(f) Recovered upper crustal anomaly, (g)–(i) recovered lower crustal anomaly, and (j)–(l) recovered Moho anomaly. Our aim is to test whether the lower crustal variation along the rift is well resolved. While the upper crustal anomalies are better recovered than those in the lower crust, the fact we resolve anomalies equally well all along the rift indicates that we are able to resolve the lower crustal variations. The velocity contours are every 0.1 km/s, the Moho contour interval is 5 km; there are no zero contours.

extended along the neovolcanic zones we would resolve such features. We therefore conclude that the anomalies do not extend to these areas.

[57] The region of low-velocity in the lower crust sits in the thickest crust on Iceland, reaching 46 km (Figure 10), and connects with low velocities in the upper crust. On top of these anomalies lies the Bárdarbunga-Grímsvötn volcanic complex, associated with the most significant volcanic events on Iceland. This complex fed the largest lava eruption witnessed by man, the Laki eruption of 1783, which produced 12–14 km^3 of basalt [*Einarsson et al.*, 1997], and has also been the most active complex during the last 100 years. The fissure swarm associated with Bárdarbunga extends over 200 km to the north and southeast from the central volcano. The large fissure eruption of Vatnaöldur in 871, located 100 km away, was fed by Bárdarbunga [*Einarsson et al.*, 1997]. Radio echo-sounding of the rock surface beneath Vatnajökull has revealed large calderas associated with both Bárdarbunga and Grímsvötn. The topography also suggests a much larger circular feature extending from the south flank of Bárdarbunga and enclosing Grímsvötn [*Bjornsson*, 1988; *Einarsson et al.*, 1997].

[58] Our lower crustal anomaly is also co-located with the center of the ~200 km diameter mantle low-velocity anomaly interpreted as a plume [*Tryggvason et al.*, 1983; *Wolfe et al.*, 1997; *Allen et al.*, 1999; *Foulger et al.*, 2000; *Allen*

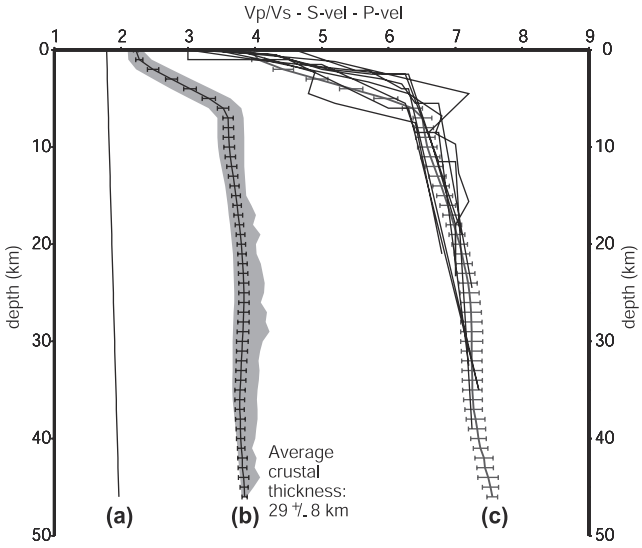

Figure 13. Average crustal velocity model for Iceland. We sample our 3-D velocity model at all points within a circle of radius 160 km centered in central Iceland. (b) The *S* velocity, indicated as an average for Iceland (solid line with standard deviation) and the full range of values observed (gray area). (c) The solid lines indicate a sample of V_P profiles from previous studies [*Bjarnason et al.*, 1993; *Staples et al.*, 1997; *Darbyshire et al.*, 1998]. (c) The gray line with error bars is V_P obtained from our average V_S using the V_P/V_S ratio indicated by Figure 13a. We find good agreement when there is a slight gradient in the V_P/V_S ratio (a), but not for a constant ratio.

et al., 2002]. The association of the mantle plume with the crustal velocity anomalies is further supported by the geochemistry of erupted lavas. *Breddam et al.* [2000] map gradients in the $^3He/^4He$ ratios along the neovolcanic zones and find the highest ratios of $^3He/^4He$ (~20 R/Ra) centered on Bárdarbunga-Grímsvötn, with declining ratios to the north and south. High $^3He/^4He$ are a classic signature of a primitive mantle plume, and *Breddam et al.* [2000] interpret the 100 km diameter plateau of high ratios as representing the lateral extent of the mantle plume. We suggest that the low-velocity anomaly extending through the entirety of the crust beneath central Iceland represents a thermal halo associated with the fluxing of magma from the core of the mantle plume to the upper crust. This gives rise to the correlation between the crustal velocity anomaly and the high $^3He/^4He$ ratios. The high degree of volcanic activity at Bárdarbunga-Grímsvötn is due to its location above this vertical region of magma flux, a pipe connecting the mantle plume to more ridge-like crustal formation processes.

[59] Our conclusions about the nature of this lower crust anomaly are very similar to those of *Tilmanm et al*. [2001]. They image a broad (~100 km) low-velocity anomaly in their *P* velocity tomography image of the lithosphere beneath Kilauea volcano in Hawaii. Thermal modeling demonstrates that it is not possible to generate such a broad anomaly by thermal conduction from a single conduit. Instead, multiple melt paths or pockets are required to heat such a broad region of the lithosphere. We suggest that a similar process is responsible for the passage of melt through the lower crust in Iceland resulting in the 150 km diameter low-velocity anomaly (Figure 9b).

[60] Similar plumbing has been imaged on the Mid-Atlantic Ridge 35°N by *Magde et al.* [2000], though on a different scale. They find two vertical low-velocity columns less than 10 km in diameter in the lower crust (>3.5 km depth) close to the center of the ridge segment studied. These low-velocity columns connect to a horizontal region of low-velocity in the upper crust extending for at least 45 km parallel to the ridge axis and 10 km perpendicular to the ridge axis. This horizontal anomaly includes pockets of even lower velocity, interpreted as magma chambers based on their location beneath volcanoes. *Magde et al.* [2000] interpret the lower crustal anomalies as pipes fluxing material through the lower crust into the horizontal ridge-parallel anomaly in the upper crust based on their location near the center of the ridge segment. The pipes feed material to the discrete magma chambers which are responsible for crustal formation. This structure is observed on a ridge segment scale.

[61] In Iceland we also see a vertical low-velocity anomaly extending through the lower crust which connects to a horizontal ridge-parallel anomaly in the upper crust. The horizontal anomaly contains broad regions of lower velocity which we argue are associated with deep (~10 km) magma sources beneath the most active volcanic complexes on Iceland. The larger scale of Iceland's plumbing, in comparison with normal mid-ocean ridge segments, is driven by the larger scale melting processes occurring beneath Iceland due to the mantle plume. This increase in scale is also observed in the surface geology. Ridge segments on Iceland, exhibited as fissure swarms, extend over 200 km in length.

5.3. V_P/V_S Ratio Through the Crust

[62] Estimates of the V_P/V_S ratio over broad regions of Iceland have ranged between 1.72 [*Tryggvason*, 1962] and 1.84 [*Palmason*, 1971]; however, controlled source wide-angle experiments over the last decade have mostly narrowed this range to 1.75 – 1.79 [*Bjarnason et al.*, 1993; *Menke et al.*, 1996; *Brandsdottir et al.*, 1997; *Staples et al.*, 1997; *Darbyshire et al.*, 1998; *Menke et al.*, 1998]. These numbers are consistent with gabbro well below the solidus, as the shear modulus drops rapidly above 800°C [*Kampfmann and Berckhemer*, 1985]. The exception to this range of values is an observation of V_P/V_S = 1.88 using a *PmP*/*SmS* travel time between a shot on the north coast in the neovolcanic zone and a station at Krafla, also in the Northern Neovolcanic Zone [*Brandsdottir et al.*, 1997]. Higher ratios are suggestive of lower *S* velocities and could be interpreted as the result of higher temperatures in the neovolcanic zone.

[63] In order to test whether our *S* velocity observations are consistent with previous *P* velocity models and the above V_P/V_S ratios we construct an average 1-D crustal velocity model from our 3-D model. We sample ICECRTb at ~10 km intervals within a circular region of radius 160 km centered on 64.9°N, 18.4°W. The velocity is averaged at each depth to produce the velocity model shown in Figure 13. Standard deviations are calculated (error bars) and the gray area represents the full range of velocities observed. Note that only crustal portions of the model are included; this is the reason for the slight reduction in velocity below ~35 km, as the thickest crust in our model is also associated with low velocities. The average crustal thickness is 29 ± 8 km.

[64] Our average velocity structure is compared with a sampling of V_P models taken from *Bjarnason et al.* [1993], *Staples et al.* [1997] and *Darbyshire et al.* [1998] by simply multiplying with a V_P/V_S ratio. It is impossible to get good agreement in both the upper and lower crust with a constant V_P/V_S ratio. We obtain a good correlation between the *P* and *S* velocity models using a slight gradient in V_P/V_S of 0.004 km^{-1} and a surface V_P/V_S of 1.78 (Figure 13). This corresponds to a V_P/V_S of 1.92 at 35 km depth, the increase being necessary to accommodate the lower velocities we observe in the thicker crust.

5.4. Crustal Thickness and Mantle Melt Production

[65] The crustal thickness of oceanic lithosphere is equivalent to the total thickness of melt generated in the asthenosphere beneath the rift. Rare Earth Element (REE) inversions [*McKenzie and O'Nions*, 1991] using the compositions of surface magmas have been very successful at estimating melt production. For example, REE predictions of melt thickness from normal mid-ocean ridge basalts are in good agreement with seismic observations of crustal thickness [*White et al.*, 1992], indicating that upwelling beneath normal ridges is a passive response to lithospheric separation. REE studies for Iceland indicate a melt thickness of 15–20 km [*White et al.*, 1995; *White and McKenzie*, 1995]; however, the average crustal thickness is 29 km. This requires active fluxing of source material through the asthenospheric melt zone by a factor of 1.5 to 2 times the passive upwelling rate. The thickest crust would require a fluxing factor as high as 3. This observation suggests that the Iceland plume is still a very active feature of North Atlantic tectonics.

[66] Clearly, the thickness of the Icelandic crust is very anomalous. While the average is 29 km, 4–5 times the remarkably constant normal oceanic crustal thickness of 6 km [*Mutter and Mutter*, 1993], the range of thicknesses is even greater, from 15 to 46 km, or 31 km in total. The thickness varies both as a function of distance from the Iceland plume and as a function of time of crustal formation. If the crustal formation process were independent of time, we would expect the same crustal thickness along plate flow lines as the crust moves away from the ridge. This is not the case; rather than a ridge of thick crust extending east-west across Iceland we see a more radial anomaly on the crustal thickness map (Figure 7d). There are three possible explanations for the time dependence of crustal thickness: (1) lower crustal flow, (2) a pulse of melt generation associated with the recent deglaciation, (3) time dependent melt generation due to temperature variations of the plume. We consider these in turn.

[67] Lower crustal flow after crustal formation would allow thick crust to develop directly above the plume, which then spreads laterally (north-south) as the crust is carried away from the rift. If this were the case, we would expect the integrated crustal thickness along any constant-time line to be the same for all times. Inspection of Figure 7d demonstrates that this is not the case.

[68] In the ~5000-year period following the end of the last glacial interval, surface volcanism on Iceland increased by a factor of 20 to 30 [*Sigvaldason et al.*, 1992]. This was due to the rapid removal of the ice-cap over ~1000 years [*Sigmundsson*, 1991], which caused decompression of the mantle beneath the ice-cap and increased fluxing through the melt zone. However, this effect is not sufficient to cause crustal thickness variations on the scale that we see. *Jull and McKenzie* [1996] estimate that the total volume of magma that could be produced by this process is 3100 km^3. If all this material were to form a cone on the base of the crust it would be a mere 25 km in radius and 5 km in height.

[69] The remaining explanation for the variations in crustal thickness is a variation in plume productivity as "blobs" of material rise through the mantle. REE inversions of basalts in Iceland's neovolcanic zones suggest a mantle potential temperature of 1450–1500°C [*White*, 1997]. At these temperatures, a 50°C change in potential temperature would result in a ~7 km increase or decrease in melt thickness for passively upwelling material [*White and McKenzie*, 1995]. This demonstrates the sensitivity of melt production and crustal thickness to relatively small changes in the potential temperature of the plume.

[70] An alternative to high temperature blobs is compositionally distinct blobs. The two-stage melting model of *Phipps Morgan and Morgan* [1999] could explain both the time variability and the along-ridge variations in crustal thickness. Easy-to-melt lumps are extracted from the rising plume, but less melt is extracted from the more depleted, MORB-like mantle remaining as residual plume material moves along the ridge away from the hot spot. Compositional variations in the easy-to-melt lumps could also cause a gradual increase in the degree of melting with time.

[71] In an effort to find other evidence for the time dependence of plume activity in Iceland we turn to *White* [1997]. He calculated residual height variations along two crustal flow lines in the North Atlantic [see *White*, 1997, Figure 6]. The residual height is the height of zero-age crust above 2.5 km below sea level, the normal water depth at oceanic spreading centers. This height is calculated from the current depth by backstripping to remove sediment thickness variations, assuming Airy isostasy and a density relationship, the effects of lithospheric cooling and sinking with age are also removed. The variations in residual height with time are a proxy for the mantle temperature, allowing us to track variations in the temperature of the Iceland plume as the plume material is funneled down the Reykjanes Ridge. The trends on the two lines are correlated and indicate a gradual decrease in plume temperature from the time of North Atlantic breakup at ~55 Ma until a minimum at 10–13 Ma. The temperatures have been rising rapidly for the last 5 Myr.

[72] These variations correlate exceptionally well with crustal thickness variations on Iceland when ridge jumps are taken into account. The oldest paleoridge on Iceland runs along the northwestern edge of the Westernfjords, and we refer to it as the northwestern rift. Ridge activity started to shift eastward from the northwestern rift to the adjacent Snæfellsnes rift at about 15 Ma [*Hardarson et al.*, 1997]. At 6.5–7 Ma the rift started to shift farther east again from Snæfellsnes to the Western Neovolcanic Zone in the south and the Northern Neovolcanic Zone in the north [*Helgason*, 1985]. Finally, at 2–3 Ma the Northern Neovolcanic Zone started to propagate south, forming the Eastern Neovolcanic Zone [*Saemundsson*, 1979].

[73] The Snæfellsnes rift zone was active from ~15 to ~5 Ma, a time period which correlates with the lowest residual height anomalies in the history of the North Atlantic, which in turn indicates a period of low plume activity.

The rift ran along the Snæfellsnes Peninsula and then turned north, running west of the Skagi Peninsula [*Hardarson et al.*, 1997]. This corresponds with some of the thinnest crust on Iceland, which wraps around the southeastern edge of the Westernfjords. The thicker crust beneath the Westernfjords is probably associated with the northwestern rift, which was active prior to the period of minimum residual height and minimum plume temperature. In northern Iceland, there are two north-south ridges of thick crust adjacent to the current Northern Neovolcanic Zone (Figure 7d). We associate the thicker ridges with a period of more active crustal formation in the north, on initiation of the Northern Neovolcanic Zone at about 7 Ma. The thin crust beneath the rift today appears to be due to reduced magma supply from the mantle plume. This is consistent with the upper crustal piping we discuss above, which extends along all of the current rift except above the region of thin crust.

[74] In south Iceland, ridges of thick crust extend along both the Western and Eastern Neovolcanic Zones, which have been active during the period of increasing temperature, since ~7 and 3 Ma, respectively. This indicates increased crustal production associated with magma supply from the plume, and the upper crustal anomalies delineate this plumbing. Finally, the thickest crust, found in central Iceland, is due to its location directly above the mantle plume during a time when the plume potential temperature experienced an increase; the potential temperature in this region remains high today.

6. Summary

1. Our 3-D crustal *S* velocity model and Moho map for Iceland, named ICECRTb, satisfies Love wave and S_n travel time constraints, and is consistent with previous observations of crustal thickness. The bulk of the information about the crustal structure comes from surface wave fitting, which is successfully applied in a higher frequency window than previously (0.03–0.1 Hz).

2. In the upper 10–15 km of crust, elongated low-velocity zones are associated with the locus of the Mid-Atlantic Ridge across Iceland. The Western and Eastern Neovolcanic zones are underlain by broad regions of low-velocity which extend north of Vatnajökull. The two most active volcanic complexes in Iceland, Hekla and Bárdarbunga-Grímsvötn, are located above *S* velocity minima of −7% which lie in the 5–10 km depth range. This is consistent with previous observations suggesting a deep magma source for these two complexes. The other three main volcanoes on Iceland (in terms of activity in historic times), Krafla, Askja, and Katla, are not associated with very low-velocities; in fact, low velocities are almost absent. Since previous work suggests these volcanoes exhibit small, shallow (~3 km) magma chambers and infrequent activity (every ~100 years), we believe that they are the product of a different, perhaps more passive, ridge-like process.

3. We suggest that the low-velocity anomalies in the Icelandic crust image the thermal halo of a plume-driven plumbing system. Material is fed from the core of the mantle plume vertically up through the lower crust in central Iceland and then laterally along the upper crustal rift system. The strongest plume-like geochemical signatures in central Iceland are the result of this direct connection from the surface to the plume core. There is an absence of the horizontal piping in the midsection of the Northern Neovolcanic Zone. This is consistent with the observed thin crust resulting from reduced flow of material from the plume.

4. A linear increase in the V_P/V_S ratio with depth from 1.78 at the surface to 1.92 at 35 km depth successfully relates our V_S observations with previous V_P measurements, while a constant V_P/V_S does not. These ratios do not suggest broad molten regions at these depths, but rather crystalline crust above the gabbro solidus. This is consistent with our plumbing hypothesis, in which material is fed through the lower crust to upper crustal magma chambers responsible for the bulk of crustal formation.

5. Comparison of the crustal thickness in Iceland with predicted melt thicknesses from REE inversions of Icelandic basalts suggests active fluxing of asthenospheric material through the melt zone. This is consistent with the presence of a buoyant plume beneath Iceland. The degree of fluxing, as recorded by the variation in crustal thickness across Iceland (15 to 46 km), has varied between factors of 1 and 3 with respect to passive upwelling due to plate separation. These large variations are the result of changes in plume potential temperature, superimposed with rift relocation on Iceland over the last ~20 Myr. The thinnest crust is associated with the Snæfellsnes rift zone, which was active during the period of lowest plume potential temperature. Plume potential temperature has risen rapidly over the last 5 Myr, resulting in the thickest crust being formed directly above the plume core today.

6. The Icelandic crust is in broad Airy-isostatic equilibrium as expected based on its recent formation at an active rift zone. The isostatic relation can be used to calculate the density ratio across the Moho, which we find to be 0.96. This ratio is higher than observed for normal parts of the Mid-Atlantic Ridge, where it is 0.90, implying either higher density lower crust or lower density upper mantle in Iceland.

[75] **Acknowledgments.** This work was funded by NSF EAR/9417918 and NERC GST/02/1238. We would like to thank Tony Dahlen for regular discussions, Paul Friberg and Sid Hellman from the IRIS-PASSCAL project for their support in the field and data handling operations, and all the Icelanders who lodged our instruments. We also thank the Associate Editor, an anonymous reviewer, and E. Debayle for insightful comments which have enhanced the manuscript. The figures were produced with GMT [*Wessel and Smith*, 1995].

References

Allen, R. M., et al., The thin hot plume beneath Iceland, *Geophys. J. Int.*, *137*, 51–63, 1999.

Allen, R. M., et al., Imaging the mantle beneath Iceland using integrated seismological techniques, *J. Geophys. Res.*, 10.1029/2001JB000595, in press, 2002.

Angenheister, G., et al., Reykjanes Ridge Iceland Seismic Experiment (RRISP 77), *Z. Geophys.*, *47*, 228–238, 1980.

Arnadottir, T., F. Sigmundsson, and P. T. Delaney, Sources of crustal deformation associated with the Krafla, Iceland, eruption of September 1984, *Geophys. Res. Lett.*, *25*, 1043–1046, 1998.

Arvidsson, R., and G. Ekström, Global CMT analysis of moderate earthquakes, $M_w \geq 4.5$, using intermediate-period surface waves, *Bull. Seismol. Soc. Am.*, *88*, 1003–1013, 1998.

Bath, M., Crustal structure of Iceland, *J. Geophys. Res.*, *65*, 1793–1807, 1960.

Beblo, M., and A. Bjornsson, A model of electrical resistivity beneath NE-Iceland, *J. Geophys.*, *47*, 184–190, 1980.

Bjarnason, I. T., W. Menke, O. G. Flovenz, and D. Caress, Tomographic image of the Mid-Atlantic plate boundary in southwestern Iceland, *J. Geophys. Res.*, *98*, 6607–6622, 1993.

Bjornsson, A., K. Saemundsson, P. Einarsson, E. Tryggvason, and

K. Groenvold, Current rifting episode in north Iceland, *Nature*, *266*, 318–323, 1977.
Bjornsson, A., G. Johnsen, S. Sigurdsson, G. Thorbergsson, and E. Tryggvason, Rifting of the plate boundary in north Iceland 1975–1978, *J. Geophys. Res.*, *84*, 3029–3038, 1979.
Bjornsson, H., Hydrology of ice caps in volcanic regions, M.Sc. thesis, Univ. of Iceland, Reykjavik, 1988.
Brandsdottir, B., and W. H. Menke, Thin low-velocity zone within the Krafla Caldera, NE-Iceland attributed to a small magma chamber, *Geophys. Res. Lett.*, *19*, 2381–2384, 1992.
Brandsdottir, B., W. Menke, P. Einarsson, R. S. White, and R. K. Staples, Faroe-Iceland Ridge Experiment 2: Crustal structure of the Krafla central volcano, *J. Geophys. Res.*, *102*, 7867–7886, 1997.
Breddam, K., M. D. Kurz, and M. Storey, Mapping out the conduit of the Iceland mantle plume with helium isotopes, *Earth Planet. Sci. Lett.*, *176*, 45–55, 2000.
Camitz, J., F. Sigmundsson, G. Foulger, C. H. Jahn, C. Volksen, and P. Einarsson, Plate boundary deformation and continuing deflation of the Askja volcano, north Iceland, determined with GPS, 1987–1993, *Bull. Volcanol.*, *57*, 136–145, 1995.
Clark, S. P., Jr., *Handbook of Physical Constants*, rev. ed., 587 pp., Geol. Soc. of Am., Boulder, Colo., 1966.
Darbyshire, F. A., I. T. Bjarnason, R. S. White, and O. G. Flovenz, Crustal structure above the Iceland mantle plume imaged by the ICEMELT refraction profile, *Geophys. J. Int.*, *135*, 1131–1149, 1998.
Darbyshire, F. A., K. F. Priestley, R. S. White, R. Stefansson, G. B. Gudmundsson, and S. S. Jakobsdottir, Crustal structure of central and northern Iceland from analysis of teleseismic receiver functions, *Geophys. J. Int.*, *143*, 163–184, 2000a.
Darbyshire, F. A., R. S. White, and K. F. Priestley, Structure of the crust and uppermost mantle of Iceland from a combined seismic and gravity study, *Earth Planet. Sci. Lett.*, *181*, 409–428, 2000b.
Das, T., and G. Nolet, Crustal thickness estimation using high-frequency Rayleigh-waves, *Geophys. Res. Lett.*, *22*, 539–542, 1995.
Du, Z. J., and G. R. Foulger, The crustal structure beneath the northwest fjords, Iceland, from receiver functions and surface waves, *Geophys. J. Int.*, *139*, 419–432, 1999.
Einarsson, P., *S*-wave shadows in the Krafla Caldera in NE-Iceland, evidence for a magma chamber in the crust, *Bull. Volcanol.*, *41*, 187–195, 1978.
Einarsson, P., B. Brandsdottir, M. T. Gudmundsson, H. Bjornsson, K. Gronvold, and F. Sigmundsson, Center of the Iceland hotspot experiences volcanic unrest, *Eos Trans. AGU*, *78*, *369*, 374–375, 1997.
Ekström, G., J. Tromp, and E. W. F. Larson, Measurements and global models of surface wave propagation, *J. Geophys. Res.*, *102*, 8137–8157, 1997.
Foulger, G. R., et al., The seismic anomaly beneath Iceland extends down to the mantle transition zone and no deeper, *Geophys. J. Int.*, *142*, F1–F5, 2000.
Gronvold, K., G. Larsen, P. Einarsson, S. Thorarinsson, and K. Saemundsson, The Hekla eruption 1980–1981, *Bull. Volcanol.*, *46*, 349–363, 1983.
Gudmundsson, O., B. Brandsdottir, W. Menke, and G. E. Sigvaldason, The crustal magma chamber of the Katla volcano in south Iceland revealed by 2-D seismic undershooting, *Geophys. J. Int.*, *119*, 277–296, 1994.
Hardarson, B. S., J. G. Fitton, R. M. Ellam, and M. S. Pringle, Rift relocation—A geochemical and geochronological investigation of a palaeo-rift in northwest Iceland, *Earth Planet. Sci. Lett.*, *153*, 181–196, 1997.
Helgason, J., Shifts of the plate boundary in Iceland: Some aspects of Tertiary volcanism, *J. Geophys. Res.*, *90*, 84–92, 1985.
Jull, M., and D. McKenzie, The effect of deglaciation on mantle melting beneath Iceland, *J. Geophys. Res.*, *101*, 21,815–21,828, 1996.
Kampfmann, W., and H. Berckhemer, High-temperature experiments on the elastic and anelastic behavior of magmatic rocks, *Earth Planet. Sci. Lett.*, *40*, 223–247, 1985.
Kjartansson, E., and K. Gronvold, Location of a magma reservoir beneath Hekla Volcano, Iceland, *Nature*, *301*, 139–141, 1983.
Linde, A. T., K. Agustsson, I. S. Sacks, and R. Stefansson, Mechanism of the 1991 eruption of Hekla from continuous borehole strain monitoring, *Nature*, *365*, 737–740, 1993.
Magde, L. S., A. H. Barclay, D. R. Toomey, R. S. Detrick, and J. A. Collins, Crustal magma plumbing within a segment of the Mid-Atlantic Ridge, 35°N, *Earth Planet. Sci. Lett.*, *175*, 55–67, 2000.
McKenzie, D., and R. K. O'Nions, Partial melt distributions from inversion of rare-earth element concentrations, *J. Petrol.*, *32*, 1021–1091, 1991.
Menke, W., Crustal isostasy indicates anomalous densities beneath Iceland, *Geophys. Res. Lett.*, *26*, 1215–1218, 1999.
Menke, W., and V. Levin, Cold crust in a hot spot, *Geophys. Res. Lett.*, *21*, 1967–1970, 1994.
Menke, W., V. Levin, and R. Sethi, Seismic attenuation in the crust at the mid-Atlantic plate boundary in Iceland, *Geophys. J. Int.*, *122*, 175–182, 1995.
Menke, W., B. Brandsdottir, P. Einarsson, and I.-T. Bjarnason, Reinterpretation of the RRISP-77 Iceland shear-wave profiles, *Geophys. J. Int.*, *126*, 166–172, 1996.
Menke, W., M. West, B. Brandsdottir, and D. Sparks, Compressional and shear velocity structure of the lithosphere in northern Iceland, *Bull. Seismol. Soc. Am.*, *88*, 1561–1571, 1998.
Mooney, W. D., G. Laske, and T. G. Masters, CRUST 5.1: A global crustal model at 5° × 5°, *J. Geophys. Res.*, *103*, 727–747, 1998.
Morgan, W. J., Convection plumes in the lower mantle, *Nature*, *230*, 42–43, 1971.
Muller, R. D., W. R. Roest, J. Y. Royer, L. M. Gahagan, and J. G. Sclater, Digital isochrons of the world's ocean floor, *J. Geophys. Res.*, *102*, 3211–3214, 1997.
Mutter, C. Z., and J. C. Mutter, Variations in thickness of layer 3 dominate oceanic crustal structure, *Earth Planet. Sci. Lett.*, *117*, 295–317, 1993.
Nettles, M., and G. Ekström, Faulting mechanism of anomalous earthquakes near Bardarbunga Volcano, Iceland, *J. Geophys. Res.*, *103*, 17,973–17,983, 1998.
Nolet, G., Partitioned waveform inversion and two-dimensional structure under the network of autonomously recording seismographs, *J. Geophys. Res.*, *95*, 8499–8512, 1990.
Palmason, G., Crustal structure of Iceland from explosion seismology, *Soc. Sci. Isl.*, *XL*, 1971.
Palmason, G., Kinematics and heat flow in a volcanic rift zone, with application to Iceland, *Geophys. J. R. Astron. Soc.*, *33*, 451–481, 1973.
Paterson, W. S. B., *The Physics of Glaciers*, Pergamon, New York, 1994.
Phipps Morgan, J., and W. J. Morgan, Two-stage melting and the geochemical evolution of the mantle: A recipe for mantle plum-pudding, *Earth Planet. Sci. Lett.*, *170*, 215–239, 1999.
Saemundsson, K., Outline of the geology of Iceland, in *Geology of Iceland*, edited by K. Saemundsson, pp. 7–28, [Iceland Glaciological Society], Reykjavik, Iceland, 1979.
Sigmundsson, F., Postglacial rebound and asthenosphere viscosity in Iceland, *Geophys. Res. Lett.*, *18*, 1131–1134, 1991.
Sigmundsson, F., P. Einarsson, and R. Bilham, Magma chamber deflation recorded by the Global Positioning System—The Hekla 1991 eruption, *Geophys. Res. Lett.*, *19*, 1483–1486, 1992.
Sigvaldason, G. E., K. Annertz, and M. Nilsson, Effect of glacier loading and deloading on volcanism—postglacial volcanic production-rate of the Dyngjufjoll area, central Iceland, *Bull. Volcanol.*, *54*, 385–392, 1992.
Smith, W. H. F., and D. T. Sandwell, Global sea floor topography from satellite altimetry and ship depth soundings, *Science*, *277*, 1956–1962, 1997.
Staples, R. K., R. S. White, B. Brandsdottir, W. Menke, P. K. H. Maguire, and J. H. McBride, Faroe-Iceland Ridge Experiment 1: Crustal structure of northeastern Iceland, *J. Geophys. Res.*, *102*, 7849–7866, 1997.
Takeuchi, H., and M. Saito, Seismic surface waves, in *Methods in Computational Physics*, edited by B. A. Bolt, pp. 217–295, Academic, San Diego, Calif., 1972.
Tilmann, F. J., H. M. Benz, K. F. Prestley, and P. G. Okubo, *P* wave velocity structure of the uppermost mantle beneath Hawaii from traveltime tomography, *Geophys. J. Int.*, *146*, 594–606, 2001.
Tryggvason, E., Crustal structure of the Iceland region from dispersion of surface waves, *Bull. Seismol. Soc. Am.*, *52*, 359–388, 1962.
Tryggvason, E., Multiple magma reservoirs in a rift-zone volcano—Ground deformation and magma transport during the September 1984 eruption of Krafla, Iceland, *J. Volcanol. Geotherm. Res.*, *28*, 1–44, 1986.
Tryggvason, E., Ground deformation in Askja, Iceland: Its source and possible relation to flow of the mantle plume, *J. Volcanol. Geotherm. Res.*, *39*, 61–71, 1989.
Tryggvason, E., Observed ground deformation at Hekla, Iceland prior to and during the eruptions of 1970, 1980–1981 and 1991, in *Internal Structure of Volcanoes and Geophysical Precursors of Eruptions*, edited by D. P. Hill et al., pp. 281–291, Elsevier Sci., New York, 1994.
Tryggvason, K., E. S. Husebye, and R. Stefansson, Seismic image of the hypothesized Icelandic hot spot, *Tectonophysics*, *100*, 97–118, 1983.
van der Lee, S., and G. Nolet, Upper mantle S velocity structure of North America, *J. Geophys. Res.*, *102*, 22,815–22,838, 1997.
Wang, Z., and F. A. Dahlen, Spherical-spline parameterization of 3-dimensional Earth models, *Geophys. Res. Lett.*, *22*, 3099–3102, 1995.

Weir, N. R. W., R. S. White, B. Brandsdottir, P. Einarsson, H. Shimamura, H. Shiobara, and R. F. Team, Crustal structure of the northern Reykjanes Ridge and the Reykjanes Peninsula, south-west Iceland, *J. Geophys. Res.*, *106*, 6347–6368, 2001.

Wessel, P., and W. H. F. Smith, New version of the Generic Mapping Tools released, *Eos Trans. AGU*, *76*, 329, 1995.

White, R. S., Rift-plume interaction in the North Atlantic, *Philos. Trans. R. Soc. London Ser. A*, *355*, 319–339, 1997.

White, R. S., and D. McKenzie, Mantle plumes and flood basalts, *J. Geophys. Res.*, *100*, 17,543–17,585, 1995.

White, R. S., D. McKenzie, and R. K. O'Nions, Oceanic crustal thickness from seismic measurements and rare-earth element inversions, *J. Geophys. Res.*, *97*, 19,683–19,715, 1992.

White, R. S., J. W. Bown, and J. R. Smallwood, The temperature of the Iceland plume and origin of outward-propagating V-shaped ridges, *J. Geol. Soc.*, *152*, 1039–1045, 1995.

Wolfe, C. J., I. T. Bjarnason, J. C. VanDecar, and S. C. Solomon, Seismic structure of the Iceland mantle plume, *Nature*, *385*, 245–247, 1997.

Zverev, S. M., I. P. Kosminskaya, G. A. Krasil, and G. G. Mikhota, Deep structure of Iceland and the Iceland-Faeroe-Shetland region based on seismic studies (NASP- 72), *Int. Geol. Rev.*, *19*, 11–24, 1977.

R. M. Allen, Department of Geology and Geophysics, University of Wisconsin-Madison, 1215 W Dayton St., Madison, WI 53706-1692, USA. (rallen@geology.wisc.edu)

B. Bergsson, P. Erlendsson, S. Jakobsdóttir, S. Ragnarsson, R. Stefánsson, and K. Vogfjörd, Vedurstofa Íslands, Bústadavegur 9, 150 Reykjavík, Iceland.

G. Ekström and M. Nettles, Department of Earth and Planetary Sciences, Harvard University, 20 Oxford Street, Cambridge, MA 02138, USA.

G. Foulger and M. Pritchard, Department of Geological Sciences, University of Durham, Science Laboratories, South Road, Durham DH1 3LE, UK.

B. Julian, U.S. Geological Survey, 345 Middlefield Road, MS 977, Menlo Park, CA 94025, USA.

W. J. Morgan and G. Nolet, Department of Geosciences, Guyot Hall, Princeton, NJ 08544, USA. (wjmorgan@princeton.edu; nolet@princeton.edu)